NASA Technical Memorandum 84646

NASA-TM-84646 19830018880

HEATING MEASUREMENTS ON SPACE SHUTTLE ORBITER MODELS WITH DIFFERENTIALLY DEFLECTED ELEVONS

William L. Wells

May 1983

NASA

National Aeronautics and
Space Administration

Langley Research Center
Hampton, Virginia 23665

HEATING MEASUREMENTS ON SPACE SHUTTLE

ORBITER MODELS WITH DIFFERENTIALLY

DEFLECTED ELEVONS

William L. Wells
NASA Langley Research Center
Hampton, Virginia

SUMMARY

The phase-change paint technique was used to make heat-transfer measurements on the windward wing/elevon area of 0.01-scale Space Shuttle Orbiter models with differentially deflected elevons. Outboard elevons were deflected windward at angles of 0°, 5°, 10°, 15°, and 20°. The inboard elevons were deflected leeward at twice the angle of the outboard elevons. The models were tested in air at Mach 6 and 10 with two flow conditions at each Mach number where the Reynolds numbers (based on model length) were 2.1 and 4.2 million, and 0.52 and 2.1 million, respectively. The models were tested at 20°, 28°, and 35° angle of attack in each test environment.

Heat-transfer coefficient contour maps indicated that at 20° and 28° angle of attack multiple chord-wise streaks of high heating occurred on the wings and sometimes extended to localized spots of high heating on the windward-deflected elevons. The effect of the "streak heating" was to extend the leading-edge region heating farther aft on the wing than was observed in the 35° angle of attack tests where the streaks were usually absent. Comparison of maximum heat-transfer coefficients on the outboard elevons showed that the heating increased with deflection angle. At the maximum deflection angle of 20°, heating was about four times the value

obtained for the undeflected elevon at Mach 10, and approximately 22 times the undeflected-elevon value at Mach 6.

SYMBOLS

c	specific heat of model material, W-s/K
h	convective heat transfer coefficient, W/m^2K
k	thermal conductivity of model material, W/m-K
L	total length of model excluding body flap, m
l	length of chord (includes elevon), m
M	Mach number, dimensionless
$N_{Re,L}$	free-stream Reynolds number, dimensionless
P	pressure, Pa
Pr	Prandtl number, dimensionless
$\dot{q}$	convective heating rate, W/m^2
r_c	recovery factor, dimensionless
T	temperature, K
$\bar{T}$	temperature ratio defined by equation (2)
t	time, s
X	centerline distance from model nose to a particular location, m
x	distance from wing leading edge along chord, m
α	thermal diffusivity of model material, m^2/s
α	model angle of attack, degrees
β	defined by equation (3)
γ	ratio of specific heats for air
δ	deflection angle of outboard elevon, degrees
ρ	density of model material, kg/m^3

Subscripts

aw   adiabatic wall

i   initial

max   maximum

o   reference

pc   phase change

t   total

δ elevon deflection-angle dependent

INTRODUCTION

The Space Shuttle Orbiter flies most of its entry trajectory at a high angle of attack (about 40°) such that the rudder is ineffective for yaw control. Yaw jets mounted near the aft end of the Orbiter are presently used to provide this control, although the fuel required to provide this function results in additional weight that could otherwise be used for payload. An unpublished study at Langley Research Center has indicated that over at least part of the entry trajectory yaw control could be achieved by differential deflection of the elevons. Differential deflection is here defined as a downward (into the wind) deflection of the outboard elevons and an upward deflection of the inboard elevons. An effective configuration considered in the study utilized downward deflected outboard elevons at an angle δ and inboard elevons deflected at an angle -2δ, but with δ different on opposite sides of the vehicle. This configuration was predicted to provide yaw control equal to the yaw jets at M=10, better control at lesser Mach numbers, and significant control at Mach numbers somewhat greater than 10. During the portion of the entry

trajectory when aerodynamic heating is significant, present flight procedures call for inboard and outboard elevon deflections to be in the same direction and through relatively small angles (up to about 6° on flights 1 through 4, (reference 1).

This paper reports on a series of wind tunnel heat-transfer tests conducted to ascertain the effect on aerodynamic heating of the orbiter elevons due to differential deflection. Heating on the wings forward of the elevons was also measured. The phase-change paint heat-transfer technique was used, and the study was restricted to the windward surface.

MODELS

A glassy-ceramic material was used to cast five one-percent-scale orbiter models. Each model had elevons that were deflected at angles different from the other four models. The five outboard deflection angles were: 0°, 5°, 10°, 15°, and 20° downward. The corresponding inboard deflection angles were: 0°, 10°, 20°, 30°, and 40° upward. To provide redundancy in heat transfer measurements, the port and starboard deflection angles were the same on each model since flow symmetry was expected. The correct geometry was maintained on the windward side of the elevons, but they were made thicker on the leeward side so that the one-dimensional heat-transfer approximation could be used in the heating analysis. Each model was made with an undeflected body flap, and a hollow stainless-steel sting was installed coaxial with the fuselage centerline at the time the model was cast. The sting also served as a conduit for leads of a thermo-couple that was cast into the material at the fuselage centerline just aft of the orbiter canopy. Photographs of the model with undeflected elevons are shown in figure 1.

SCOPE OF TESTS

The tests were conducted in air in two wind tunnels: the 20-Inch Mach 6 Tunnel and the Continuous Flow Hypersonic (M=10) Tunnel, both at the Langley Research Center. Each model was tested in two flow environments characterized by the free-stream Reynolds number. Nomimal free-stream Reynolds numbers at Mach 10 were 0.52 and 2.10 million, and at Mach 6, 2.10 and 4.20 million. Pertinent test conditions for all flow environments of interest are listed in Table I. Each model was tested at angles of attack of 20°, 28°, and 35° in each flow environment. The models were injected into the test stream at the desired angle of attack after tunnel flow conditions were established.

WIND TUNNELS

The Langley 20-Inch Mach 6 Tunnel is a blowdown wind tunnel that uses dry air as the test gas. The air is heated to the desired total temperature by electrical resistance heaters. A fixed-geometry, two-dimensional, contoured nozzle is used. The side walls are parallel, forming a 52 cm by 51 cm test section. A description of this facility and calibration data can be found in references 2, 3, and 4.

The Langley Continuous Flow Hypersonic Tunnel was used in a blowdown mode for the test series reported here. This tunnel also uses dry air which is heated to the total temperature by electrical resistance heaters. The three-dimensional, rectangular nozzle expands to a test section that is 79 cm square by 86 cm long. This facility is described in reference 5.

HEAT-TRANSFER MEASUREMENT TECHNIQUE

The phase-change paint technique employs a series of paints that melt, or change phase, at known temperatures. Typically, a thin coat of

light-colored paint is sprayed on a dark-colored model. The unmelted paint is opaque but becomes transparent when melted. Knowledge of the model material properties, the time required to melt the paint, and the paint melt-temperature provides sufficient information to determine the heat-transfer coefficient at a particular location. Reference 6 presents a comprehensive discussion of this technique. Only those portions that are directly applicable to this study are briefly discussed here.

Mathematical relations sufficient to determine the heat transfer coefficient can be derived from the equations governing transient one-dimensional heat conduction into a semi-infinite slab. These derived relations are

$$\bar{T} = 1 - e^{\beta^2} \text{ erfc } \beta \tag{1}$$

where
$$\bar{T} = \frac{T_{pc} - T_i}{T_{aw} - T_i} \tag{2}$$

and
$$\beta = \frac{h}{k}\sqrt{\alpha\, t} \qquad \text{or} \qquad h = \beta\sqrt{\frac{\rho c k}{t}} \tag{3}$$

The model material properties parameter $\sqrt{\rho c k}$ was experimentally determined by use of the heating device described in reference 7, β was found from equations (1) and (2), and the time t required to melt the paint at a particular location was determined from motion-picture film exposed during a test. The adiabatic wall temperature in equation (2) was obtained from

$$T_{aw} = \frac{T_{aw}}{T_t}\, T_t = \frac{1 + r_c\,(\frac{\gamma-1}{2})M^2}{1 + (\frac{\gamma-1}{2})M^2}\, T_t = \frac{1 + \sqrt{Pr}\,(\frac{\gamma-1}{2})M^2}{1 + (\frac{\gamma-1}{2})M^2}\, T_t \tag{4}$$

which assumes a constant property, laminar boundary layer flow condition. The total temperature T_t was obtained from wind-tunnel thermocouples, and the model initial temperature T_i was measured by the thermocouple that was imbedded in the model when it was cast. Enough time was allowed between tests for T_i to return to the ambient temperature.

For a particular test, a paint was selected with a phase-change temperature that would allow the data to be obtained before the thermal diffusion time was exceeded in the thinnest wall section of the model. This requirement derives from a boundary condition imposed on the original semi-infinite slab approximation. The diffusion time in the thinnest section, which was at the elevon hinge line, was about 12 seconds. Most test times were on the order of 10 seconds. Thicker sections could have accommodated longer test times. On the other hand, care was taken not to compromise data accuracy by selecting a melt temperature so low that $(T_{pc}-T_i)$ in equation (2) would be very small or that the model injection time, when conditions are transient, would be a large portion of the data gathering time at any particular location on the model. In some instances it was necessary to use a paint on the elevons with melt-temperature different from the rest of the model.

The motion-picture camera used to record the data was operated at a rate of 10 frames per second. A stroboscopic lamp was used to illuminate the model, and the pulse rate was synchronized with the camera framing rate. Continuous operating high-intensity lamps can add a significant radiant heat load to the model (ref. 6).

DATA REDUCTION AND ACCURACY

From images recorded on motion picture film, the boundary between melted and unmelted paint at a particular time during a test was superimposed on an outline of the orbiter model. This boundary represents a contour line of constant heating rate that is determined by the heat-transfer measurement technique previously discussed. At a later test time the new melt boundary, representing a lesser heating rate, was also

superimposed onto the Orbiter outline, and so on, until a heating-rate contour map of the windward wing and elevon surfaces was obtained. The area between two contour lines has heating rates that have upper and lower limits defined by the two lines. The data presented here are in terms of the heat-transfer coefficient that has been nondimensionalized by the theoretical stagnation-point coefficient (ref. 8) for a 0.305 m (1-ft) radius sphere at the model scale and test conditions.

Factors that affect the data accuracy are discussed at length in reference 6. These factors are too numerous and variable to elaborate on in this paper but include model injection time, time at which data is read, $(T_{pc}-T_i)$, known value of T_{pc}, model material properties, and determination of initial time of heating (t=0). Model illumination, camera viewing angle, and the heating gradient over a particular surface area were also found to affect the accuracy with which the data could be read from the film. Rather than try to evaluate each factor and its contribution to errors, the present phase-change data was compared to theory (ref. 9) for the same configuration and test conditions, and also to experimentally-obtained thermocouple data (ref. 10) for very nearly the same conditions. Figure 2 presents a comparison of the different methods for the orbiter fuselage centerline at $\alpha = 35°$. The methods can be seen to agree within about 5 percent over most of the data span, and only when data read times are short (at highest h/h_o) does theory and phase-change data disagree by about 10 percent. Thermocouple and phase-change data continue in close agreement throughout the data range.

RESULTS AND DISCUSSION

The highest heating rate for any case occurred along the leading edge of the wings and along the inboard edge of the outboard elevons. Values of

heating rate were not obtained in these localized areas because the paint melted almost immediately upon entry into the test stream. Furthermore, these areas soon developed a thin char layer that resulted in unknown material properties. The inboard elevons that were deflected leeward never received enough heating to melt the paint. The inboard elevons and wings were always painted with the same paint for a particular test. The outboard elevons sometimes required paint with a higher melting temperature so that the wing and elevon paint melt times would both fall within the limit specified by the data analysis technique.

Geometric patterns of heating over the wings and outer elevons were often complex. At Mach 6 the highest heating (excluding the leading edge) sometimes occurred at a spot near the center of the wing. In many other instances, at both Mach 6 and Mach 10, high heating occurred in multiple chord-wise streaks on the wings, and these streaks often extended to spots of high heating on the windward deflected elevons. Examples of multiple-streak and spot heating patterns are shown by single frames of motion-picture film in figure 3. The dark areas indicate melted paint and areas of high heating (except for shadows as indicated).

Values of heat-transfer coefficient and geometrical patterns of heating over the wing and outer elevon obtained from the Mach-6 tests are shown in figures 4 through 8. The data are shown for only one side of the model since the heating was symmetrical about the model centerline. The data are presented as ranges of nondimensionalized heat-transfer coefficients that are within a certain outlined area on the wing or elevon. The data are shown for nominal $N_{Re,L} = 2.1 \times 10^6$ and 4.2×10^6.

Consider the data for $N_{Re} = 2.1 \times 10^6$, which is the left side of each figure. When $\alpha = 35°$ and the elevons are not deflected (fig. 4(a)), the heat-transfer coefficient patterns are simple and heating decreases in a direction approximately normal to the wing leading edge. When $\alpha = 28°$ and $20°$ (figs. 4(b), 4(c)), however, chordwise streaks of high heating develop on the wing and extend across the outboard elevon. There is little apparent effect on wing heating patterns when the elevons are deflected through any angle δ (compare (a) parts of figs. 4-8) when $\alpha = 35°$, but apparently some feature in the flow structure intersects the windward-deflected elevon which results in localized spots of high heating on that surface. The most dramatic evidence of this can be seen in figure 7(a). The nature of the flow structure responsible for the streaks or spots of high heating is not known at this time, but it is thought to originate with interaction of shocks from the bow, strake, and wing. When $\alpha = 28°$ or $20°$ the multiple streaks in the heating patterns become less apparent as δ is increased. In any case, the "streak" heating was much more prominent at $\alpha = 28°$ and $20°$ than at $\alpha = 35°$.

The right side of figures 4 through 8 show the heating patterns for $N_{Re,L} = 4.2 \times 10^6$. In figures 4(a), (b), and (c), where the elevons are undeflected, the most prominent features are the spots of highest heating in the center of the wing (recall that heating at the immediate leading edge of the wing and the inside edge of the outboard elevon are not included in the data). This spot of high heating is altered by the deflection of the elevons and in most cases the highest heating then occurs on the outboard elevon. This elevon heating tends to be highest near the hinge line and extend across the width of the elevon rather than in highly localized areas as was evident in the lower Reynolds number data.

Values of heat-transfer coefficient and geometrical patterns of heating over the wing and outer elevon obtained from the Mach-10 tests are shown in figures 9 through 13. The Reynolds number for the left-hand side of each figure is 0.52×10^6, and for the right-hand side it is 2.1×10^6. Chordwise streaks of heating do not appear on the wings when $\alpha = 35°$, but they do appear when $\alpha = 28°$ or $20°$, and the greatest effect is seen at $\alpha = 20°$ (compare parts (a), (b), and (c) in any of figs. 9-13). When $\alpha = 35°$, localized spots of high heating do not appear on the outboard elevon until it is deflected $20°$, and then only for the higher Reynolds number. At $\alpha = 28°$ or $20°$, however, these high heating spots are much more common, particularly at the highest N_{Re} and lowest α. It is interesting to note that the heating patterns on the wing are not altered significantly by the elevon deflections at any particular test condition (compare the (a) parts, (b) parts, or (c) parts of figs. 9-13).

The information in figures 4 through 13 represents the basic data. Data in this form provide details of the geometric distribution of heating and may give clues as to the nature of the flow giving rise to the heating rates on various areas. However, it is difficult to identify trends in magnitude of heating rate on the wing and elevon resulting from differential deflections of the elevons. These trends can best be displayed by graphical representation of the data. For the purpose of data presentation, the wing surface is considered to be made up of four panels and the outboard elevon one panel. The location of these panels are shown in figure 14.

The effect of angle of attack and elevon deflection on maximum heating on a particular panel at M=6 is shown in figures 15 through 17. The maximum (h/h_0) was selected from any area of a particular panel provided

that value covered as much as approximately 5 percent or more of the total

panel area. The data were taken from the original (h/h_0) contour maps

corresponding to figures 4 through 8. The original figures are larger and

somewhat more detailed than figures 4 through 8. Figure 15 shows the

maximum (h/h_0) on each panel as a function of α when the elevons are not

deflected. On most panels at each α, $(h/h_0)_{max}$ for $N_{Re} = 4.2 \times 10^6$

is about twice the value for $N_{Re} = 2.1 \times 10^6$. The outboard elevon

heating, however, is not as sensitive to N_{Re} when $\alpha = 20°$ or $28°$. Except

for panel 1, the lower N_{Re} heating is greatest when $\alpha = 28°$, but in most

cases heating continually increases with α at the higher N_{Re}. The effect

of elevon deflection on the heating of the wing panels is shown in figure

16. In this plot the maximum heat-transfer coefficient on a panel that

occurred when the outboard elevon was deflected at some angle δ, is

compared to the maximum heat-transfer coefficient on that panel when the

elevon was undeflected, but at the same α and test conditions. Heating on

the most inboard panel (4) was usually the lowest, and in many tests paint

on that panel did not melt within the allotted test time. Furthermore,

panel 4 did not exhibit the spots or streaks of high heating often seen on

the other wing panels. Consequently, the panel 4 data are limited but

probably are representative of the random scatter (about $\pm$ 15 percent) in

all the data of figure 16. Except for one case, on panel 2, none of the

data for any wing panel obtained when the elevons were deflected differs

from $h_{\delta=0}$ data by more than $\pm$ 40 percent.

The effect of elevon deflection on heating of the outboard elevon

itself is much more profound than on any of the wing panels. The

comparison of maximum h for the deflected and undeflected elevon is shown

in figure 17. These data have been averaged over all α and N_{Re} since no

obvious correlation between the parameters was discernable. The spread of the data is indicated by brackets. On average, h_δ is no more than 50 percent greater than $h_{\delta=0}$ up to $\delta=10°$. Beyond that deflection, however, h_δ increases rapidly until it is as much as 22 times $h_{\delta=0}$ when $\delta=20°$.

Data from the Mach-10 tests are shown in figures 18 through 21. The maximum values of (h/h_o) found anywhere on a particular panel are shown as a function of angle of attack in figure 18 for all five panels. These data are for nominal Reynolds numbers of 0.52×10^6 and 2.1×10^6, and are from the undeflected elevons tests. Reynolds number effects are small on the wing panels, but on the outboard elevon $(h/h_o)_{max}$ is greater for the higher N_{Re} at all α. The effect of elevon deflection on heating of the wing panels is shown in figure 19. Heating of panels 1 and 4 is not greatly affected by the change in δ, as might be expected, because of their locations. Panels 2 and 3 show more variation of $(h_\delta/h_{\delta=0})_{max}$ with δ although the variation with α (indicated by different symbols) seems more evident. To show the trend in $(h/h_o)_{max}$ as a function of α for all four wing panels, the data for all δ and both N_{Re} were plotted and a curve faired through each set of data. These faired-data curves along with one theoretical curve calculated for a point at $X/L = 0.7$ on the fuselage centerline are shown in figure 20. The curves for panels 1 and 4, and the theoretical curve show a linear decrease in $(h/h_o)_{max}$ as α is decreased. Curves for panels 2 and 3 show a similar decrease when α is large ($28° < \alpha < 35°$), but $(h/h_o)_{max}$ does not continue to decrease, and even begins to rise somewhat as α decreases from $28°$ to $20°$. Although values of $(h/h_o)_{max}$ on panels 2 and 3 do not exceed the values for panel 1, the larger values at lower α may be important in terms of total heat load on the wing for flight missions that

require greater cross-range and, therefore, smaller α than has previously been flown. Apparently the high-heating streaks observed in this study at the lower α extend the high heating levels that normally occur near the wing leading edge farther back on the wing surface.

The effect of δ on $(h/h_o)_{max}$ for the outboard elevon at Mach 10 is shown in figure 21. Recall that $(h/h_o)_{max}$ for $\delta=0$ on this panel (5) was shown in figure 18. To obtain the curve in figure 21 the data were averaged over all α and N_{Re}. The data band is indicated by brackets. The values of $(h/h_o)_{max}$ increase with increasing δ and approximately double for each 10° increase in δ. These Mach-10 data are within 33 percent of the Mach-6 data up to $\delta=15°$, but the Mach-6 data are much higher at $\delta=20°$ (compare figs. 21 and 17, but note the scale difference).

COMPARISON TO FLIGHT

The nondimensionalized heating rate along a chord at approximately 80-percent semispan is shown in figure 22 for the undeflected-elevon wind-tunnel model and the STS-2 (flight) orbiter. The flight heating rate was obtained from orbiter thermocouple data and use of the computational procedure outlined in references 11, 12, and 13. The flight reference-heating rate to the stagnation point of a full-scale 0.305 m (1-ft.) radius sphere was obtained from the computational procedure of reference 14 which considers the equilibrium chemistry that is important in flight. A wall temperature of 1111 K was used in the computation. The flight and wind-tunnel conditions are shown on the figure, where M, α, and δ are very nearly the same, but the flight $N_{Re,L}$ is about three times the wind-tunnel value. Values of wind-tunnel $\dot{q}$ would be on the order of 30 percent greater at the higher (flight) $N_{Re,L}$ based on the $\alpha = 35°$ data of Fig. 18. This Reynolds number correction provides almost perfect agreement between flight and wind-tunnel data over the first 55

14

percent of the chord. In flight, transition to turbulent flow apparently occurs at about 55-percent chord so that the heating rate increases over the remainder of the chord, whereas the wind-tunnel values continue to decrease over that same length. Obviously, application of any wind-tunnel data to a flight situation requires careful consideration of the relative flow environments.

CONCLUDING REMARKS

The phase-change paint technique was used to make heat transfer mesurements on five Space Shuttle Orbiter models with differentially deflected elevons. The outboard elevons were deflected windward through an angle δ when the inboard elevons were deflected through an angle -2δ, where $\delta = 0°$, $5°$, $10°$, $15°$, and $20°$. The models were tested in air at Mach 6 and Mach 10 with two different flow conditions at each Mach number. Each test was run at three angles of attack; $20°$, $28°$, and $35°$. This study was restricted to the windward side of the wing/elevons area. Based on these tests, and restricted to this range of study, the following concluding remarks are made.

The highest heating always occurs on the wing leading edge and at the inboard edge of the outboard, windward-deflected elevon. Geometric patterns of heating on the wing and windward-deflected elevons are often complex, particularly at $20°$ and $28°$ angles of attack. Multiple chordwise streaks of higher heating often occur across the wing and sometimes extend to spots of highly localized heating on the windward-deflected elevon. In general, deflection of the elevons do not strongly alter these heating patterns on the wing. High heating near the leading edge of the wing is extended farther aft on the wing by the "streak" phenomena. In most cases deflection of the elevons does not change the maximum heat-transfer

15

coefficient anywhere on the wing by more than 40 percent of the values obtained where the elevons are undeflected at the same test condition and angle of attack. However, the maximum heat-transfer coefficient on the windward-deflected elevon is a strong function of the deflection angle. For example, when data obtained in these tests were averaged over both test conditions and all angles of attack at each Mach number, the maximum heat-transfer coefficient on the 15° deflected elevon was approximately three times the value obtained on the undeflected elevon. Furthermore, multiplying factors for the coefficient between the undeflected and 20° deflected elevon were 4 at Mach 10 and 22 at Mach 6.

REFERENCES

1. Findlay, J. T., and Compton, H. R., "On the Flight Derived/Aerodynamic Data Base Performance Comparisons For the NASA Space Shuttle Entries During the Hypersonic Regime," AIAA Paper No. 83-0115, 1983.

2. Miller, C. G., III, and Gnoffo, P. A., "Pressure Distributions and Shock Shapes for 12.84°/7° On-Axis and Bent-Nose Biconics in Air at Mach 6," NASA TM 83222, 1981.

3. Goldberg, Theodore J.; and Hefner, Jerry N. (appendix by James C. Emery), "Starting Phenomena for Hypersonic Inlets With Thick Turbulent Boundary Layers at Mach 6," NASA TN D-6280, 1971.

4. Keyes, J. Wayne, "Force Testing Manual for the Langley 20-Inch Mach 6 Tunnel," NASA TM-74026, 1977.

5. Shaefer, W. T., Jr., "Characteristics of Major Active Wind Tunnels at the Langley Research Center," NASA TM X-1130, 1965.

6. Jones, R. A., and Hunt, J. L., "Use of Fusible Temperature Indicators For Obtaining Quantitative Aerodynamic Heat-Transfer Data," NASA TR R-230, February 1966.

7. Creel, T. R., Jr., "A Device For Rapid Determination of Thermophysical Properties of Phase-Change Wind-Tunnel Models," NASA TM X-3421, 1976.

8. Fay, J. A., and Riddell, F. R., "Theory of Stagnation Paint Heat Transfer in Dissociated Air," <u>Journal of Aeronautical Sciences</u>, Vol. 25, No. 2, February 1958, pp. 73-85, 121.

9. Hamilton, H. H., "Approximate Method of Predicting Heating on the Windward Side of Space Shuttle Orbiter and Comparisons with Flight Data," AIAA Paper No. 82-0823, June 1982.

10. Herrera, B. J., "Results From a Convective Heat Transfer Rate Distribution Test on a 0.0175 Scale Model (22-0) of the Rockwell International Vehicle 4 Space Shuttle Configuration in the AEDC-VKF Tunnel B (OH49B)," Volume 1 of 2, NASA CR-147,626, 1976.

11. Pittman, C. M and Brinkley, K. L., "One-Dimensional Numerical Analysis of the Transient Thermal Response of Multilayer Insulative Systems," NASA TM X-3370, 1976.

12. Bradley, P. F. and Throckmorton, D. A., "Space Shuttle Orbiter Flight Heating Rate Measurement Sensitivity to Thermal Protection System Uncertainties," NASA TM 83138, 1981.

13. Wells, W. L. and Hudgins, J., "Experimental Assessment of a Computer Program Used in Space Shuttle Orbiter Entry Heating Analyses," NASA TM 84572, 1983.

14. Hamilton, H. Harris, II, "Approximate Method of Calculating Heating Rates at General Three-Dimensional Stagnation Points During Atmospheric Entry," NASA TM 84580, 1982.

TABLE I. NOMINAL VALUES OF WIND-TUNNEL PARAMETERS.

M	N_{RE}	T_T	T_{STATIC}	P_T	P_{STATIC}
-	(M^{-1})	(K)	(K)	(KPA)	(KPA)
6	6.56×10^6	500	62	827.4	0.55
6	13.12×10^6	506	62	1723.7	1.09
10	1.64×10^6	1011	52	2413.2	0.076
10	6.56×10^6	1011	50	10066.3	0.214
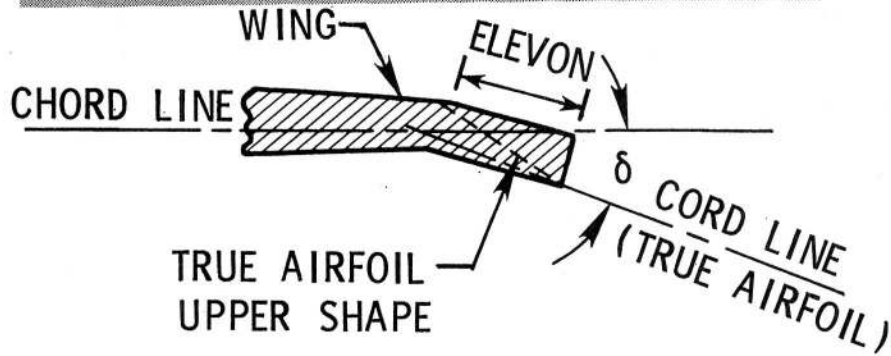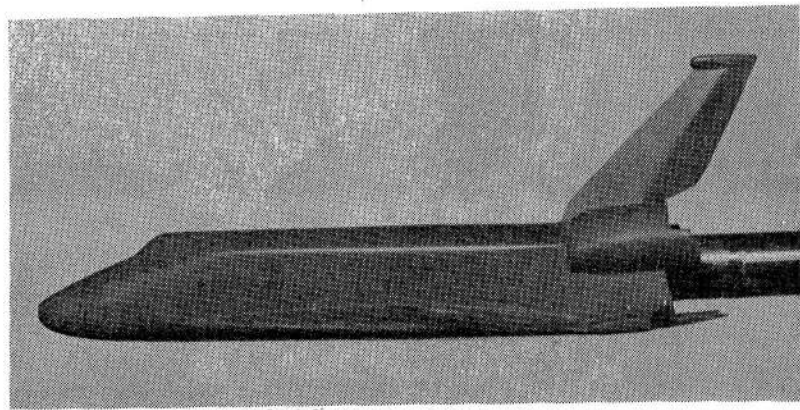
(a) Side view and definition of δ.
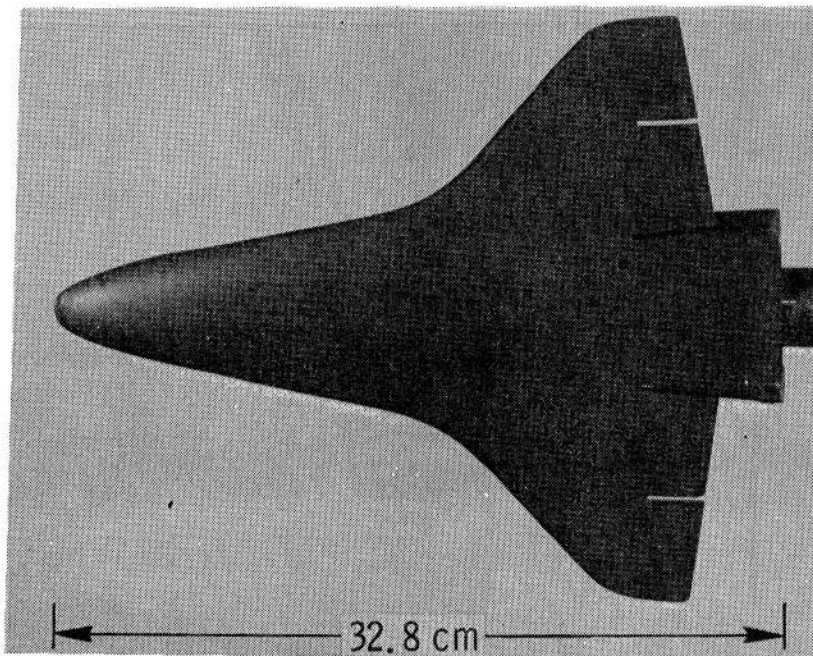
(b) Bottom view.

Figure 1.- Photographs of typical model. Undeflected elevons configuration shown (δ = 0). Side view includes sketch of wing-elevon section that defines δ.

19

MODEL SCALE	M	$N_{Re,\infty}$ m^{-1}	DATA	SOURCE
● 0.0100	9.9	1.64×10^6	PHASE-CHANGE PAINT	LANGLEY CFHT
□ 0.0175	7.9	1.77×10^6	THERMOCOUPLE	REF. 10
—— 0.0100	9.9	1.64×10^6	THEORY	REF. 9

$\alpha = 35°$

$\left(\dfrac{h}{h_0}\right)_\text{¢}$

X/L
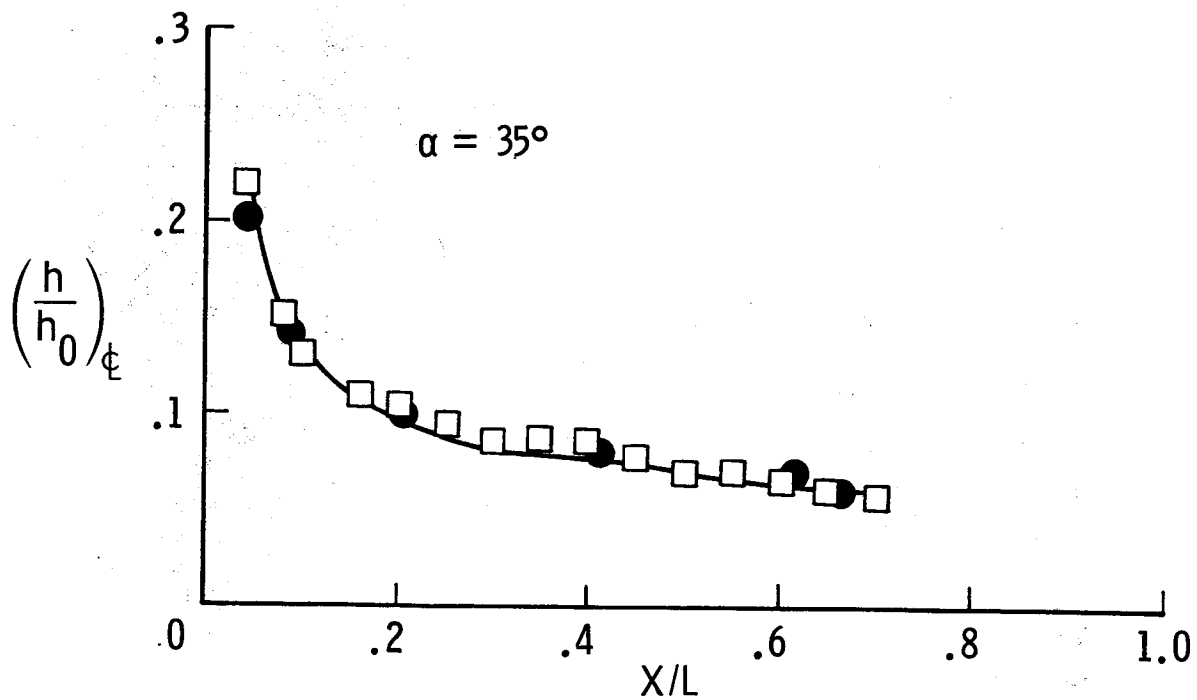
Figure 2.- Comparison of data obtained from theory and the experimental techniques of phase-change paint and thermocouples on thin metal skin along the Orbiter centerline.
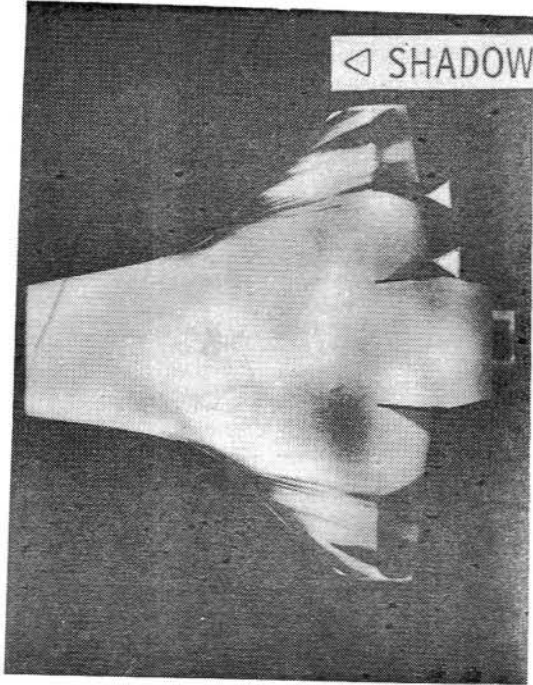
(a) M = 6
$N_{Re,L} = 2.10 \times 10^6$
$\alpha = 28°$
$\delta = 5°$
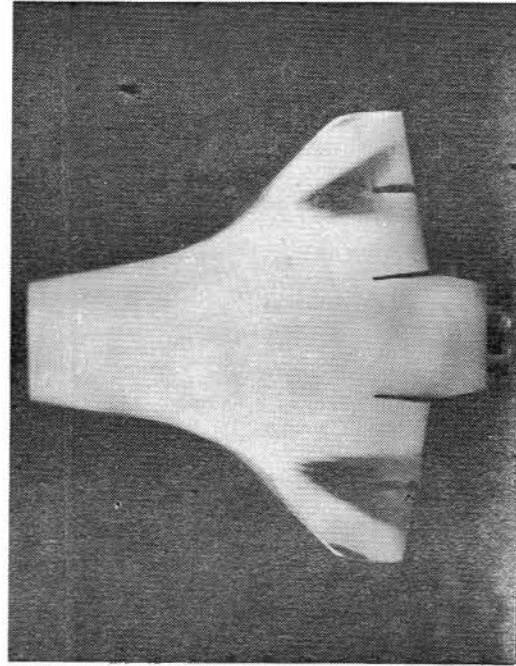
(b) M = 6
$N_{Re,L} = 4.20 \times 10^6$
$\alpha = 35°$
$\delta = 0°$
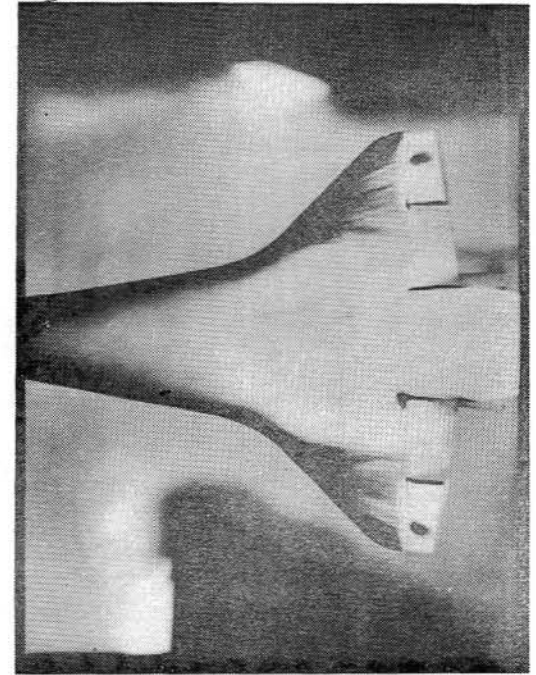
(c) M = 10
$N_{Re,L} = 2.10 \times 10^6$
$\alpha = 28°$
$\delta = 15°$

Figure 3.- Single frames of motion pictures showing examples of paint melt patterns. Dark areas indicate melted paint.

$N_{Re,L} = 2.06 \times 10^6$

$h_0 = 0.099 \ W/cm^2 K$

1	h/h_0	> 0.387
2	$0.387 > \ h/h_0$	> 0.274
3	$0.387 > \ h/h_0$	> 0.137
4	$0.274 > \ h/h_0$	> 0.193
5	h/h_0	> 0.158
6	$0.193 > \ h/h_0$	> 0.158
7	$0.158 > \ h/h_0$	> 0.137
8	$0.137 > \ h/h_0$	> 0.122
9	$0.122 > \ h/h_0$	
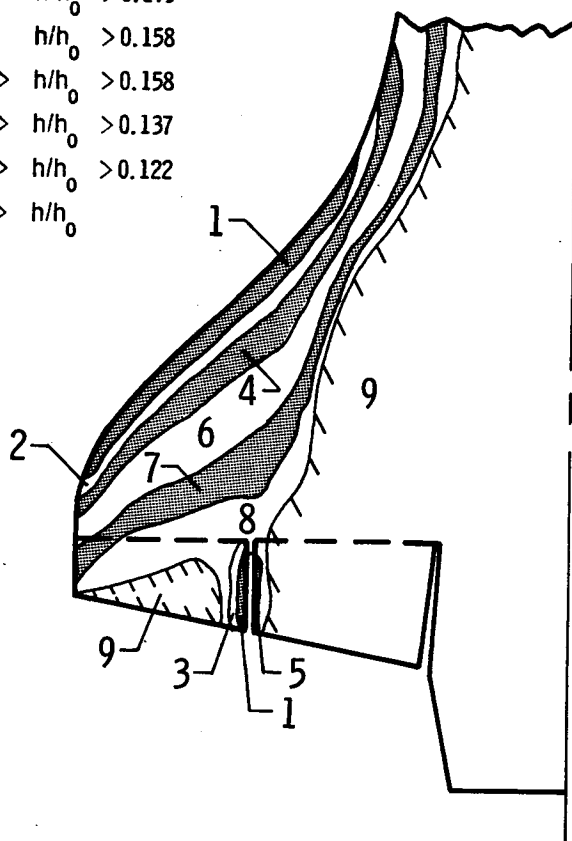
$N_{Re,L} = 4.29 \times 10^6$

$h_0 = 0.140 \ W/cm^2 K$

1	h/h_0	> 0.612
2	$0.612 > \ h/h_0$	> 0.500
3	$0.500 > \ h/h_0$	> 0.353
4	$0.353 > \ h/h_0$	> 0.274
5	$0.274 > \ h/h_0$	> 0.250
6	$0.250 > \ h/h_0$	
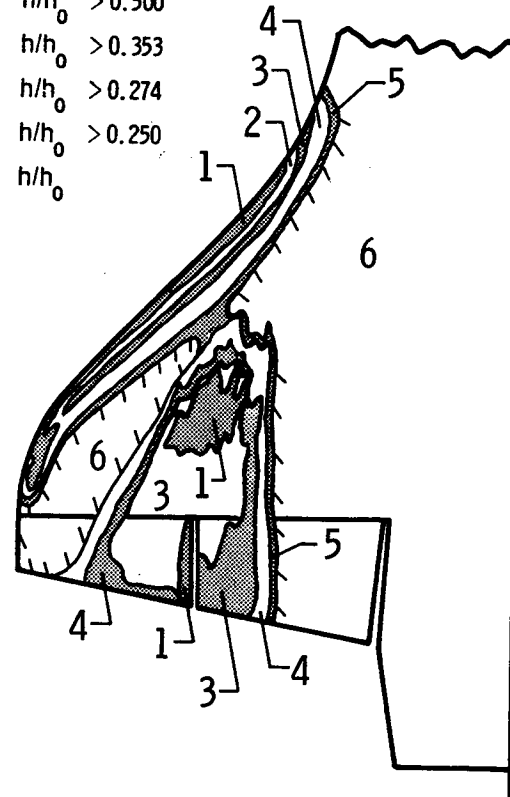
(a) $\alpha = 35°$.

Figure 4.- Heat-transfer coefficients and heating patterns on the orbiter wing and elevons at $\delta = 0$ and M = 6.
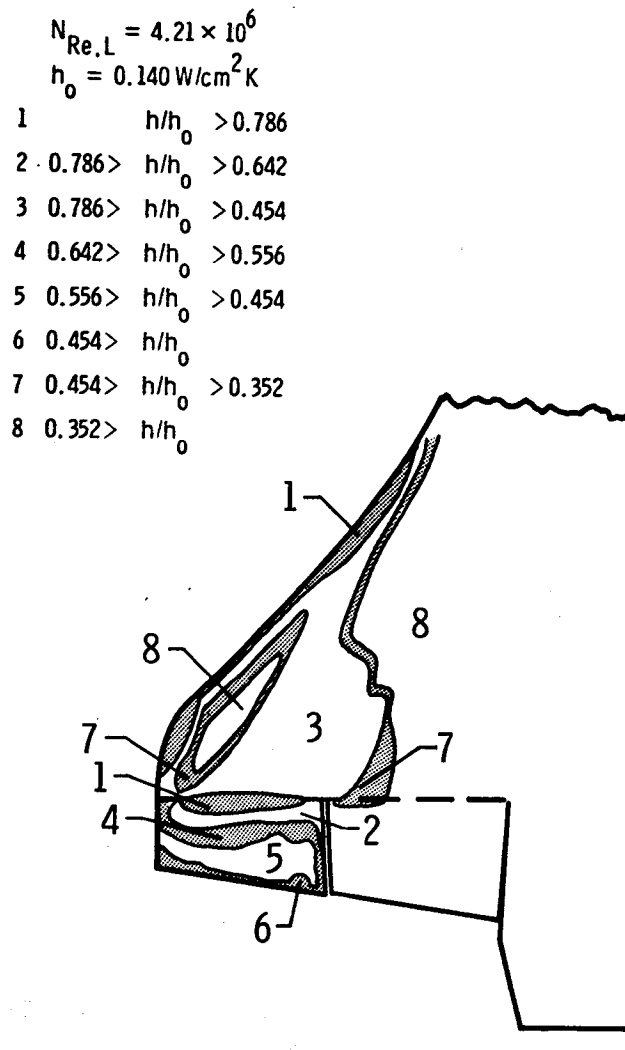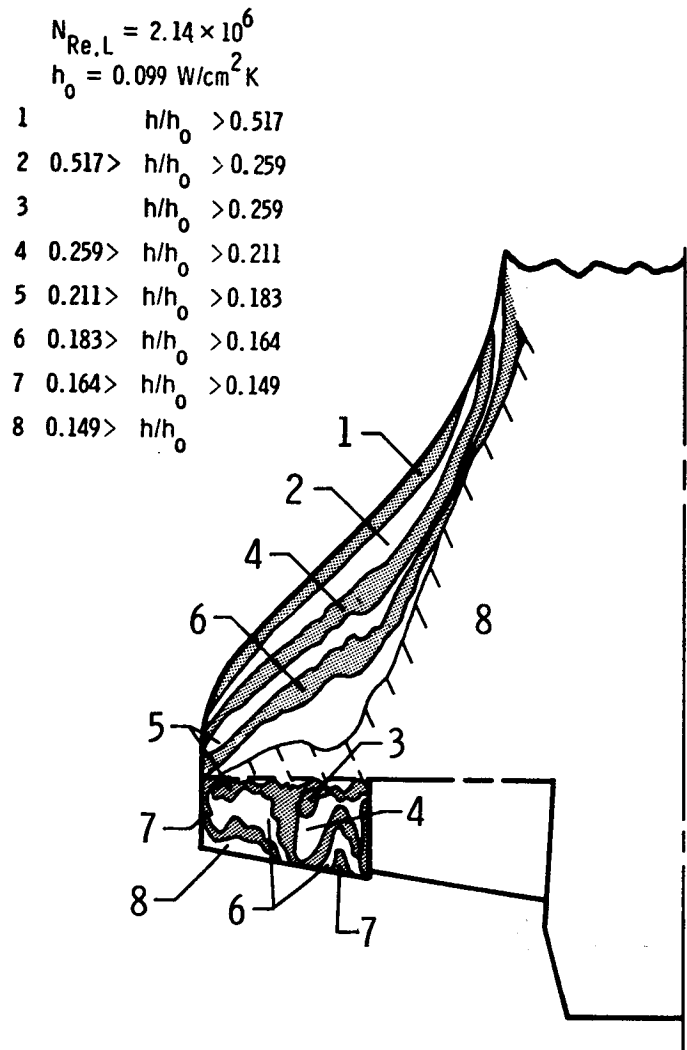
4(a)

$N_{Re,L} = 2.17 \times 10^6$

$h_0 = 0.101 \text{ W/cm}^2\text{K}$

1		h/h_0	> 0.392
2	$0.392 >$	h/h_0	> 0.196
3		h/h_0	> 0.196
4	$0.196 >$	h/h_0	> 0.160
5	$0.196 >$	h/h_0	> 0.139
6	$0.160 >$	h/h_0	> 0.139
7		h/h_0	> 0.139
8	$0.139 >$	h/h_0	> 0.113
9	$0.113 >$	h/h_0	
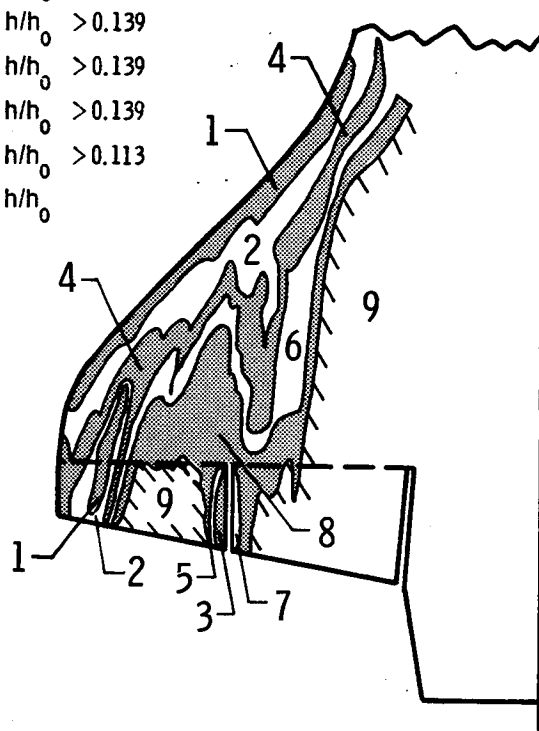
$N_{Re,L} = 4.25 \times 10^6$

$h_0 = 0.140 \text{ W/cm}^2\text{K}$

1		h/h_0	> 0.492
2	$0.492 >$	h/h_0	> 0.426
3	$0.426 >$	h/h_0	> 0.348
4	$0.348 >$	h/h_0	

(b) $\alpha = 28°$

Figure 4.- Continued.

4(8)

$N_{Re,L} = 2.21 \times 10^6$

$h_o = 0.100 \text{ W/cm}^2\text{K}$

1		h/h_o	> 0.220
2	$0.220 >$	h/h_o	> 0.110
3	$0.110 >$	h/h_o	> 0.078
4	$0.078 >$	h/h_o	

$N_{Re,L} = 4.25 \times 10^6$

$h_o = 0.140 \text{ W/cm}^2\text{K}$

1		h/h_o	> 0.590
2	$0.590 >$	h/h_o	> 0.417
3	$0.417 >$	h/h_o	> 0.295
4	$0.295 >$	h/h_o	> 0.186
5	$0.186 >$	h/h_o	

(c) $\alpha = 20°$.

Figure 4.- Concluded.

4(c)

$N_{Re,L} = 2.14 \times 10^6$

$h_0 = 0.099 \ W/cm^2 K$

1		h/h_0	> 0.517
2	$0.517 >$	h/h_0	> 0.259
3		h/h_0	> 0.259
4	$0.259 >$	h/h_0	> 0.211
5	$0.211 >$	h/h_0	> 0.183
6	$0.183 >$	h/h_0	> 0.164
7	$0.164 >$	h/h_0	> 0.149
8	$0.149 >$	h/h_0	

$N_{Re,L} = 4.21 \times 10^6$

$h_0 = 0.140 \ W/cm^2 K$

1		h/h_0	> 0.786
2	$0.786 >$	h/h_0	> 0.642
3	$0.786 >$	h/h_0	> 0.454
4	$0.642 >$	h/h_0	> 0.556
5	$0.556 >$	h/h_0	> 0.454
6	$0.454 >$	h/h_0	
7	$0.454 >$	h/h_0	> 0.352
8	$0.352 >$	h/h_0	
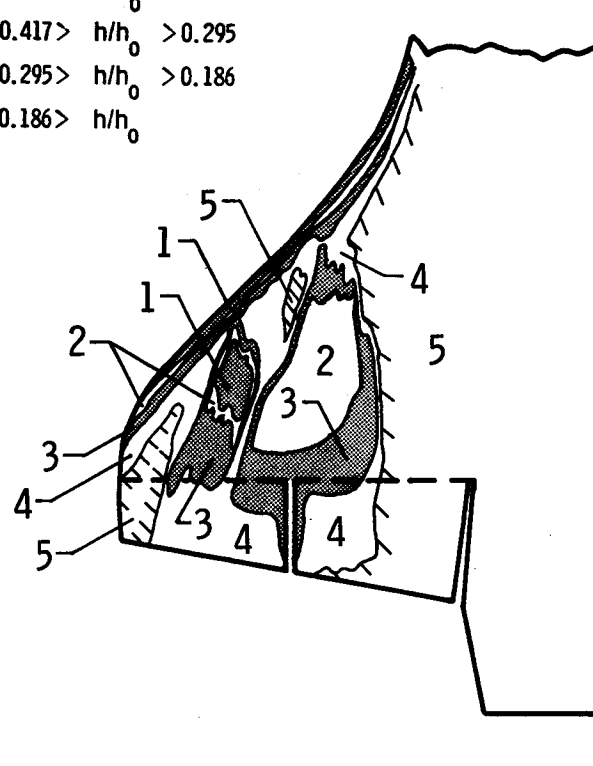
(a) $\alpha = 35°$

Figure 5.- Heat-transfer coefficients and heating patterns on the orbiter wing and elevons at $\delta = 5$ and M = 6.

5(a)

$N_{Re,L} = 2.03 \times 10^6$

$h_0 = 0.099 \, W/cm^2 K$

1          $h/h_0 > 0.352$

2 $0.352 > h/h_0 > 0.176$

3 $0.176 > h/h_0 > 0.125$

4 $0.125 > h/h_0 > 0.111$

5 $0.111 > h/h_0$
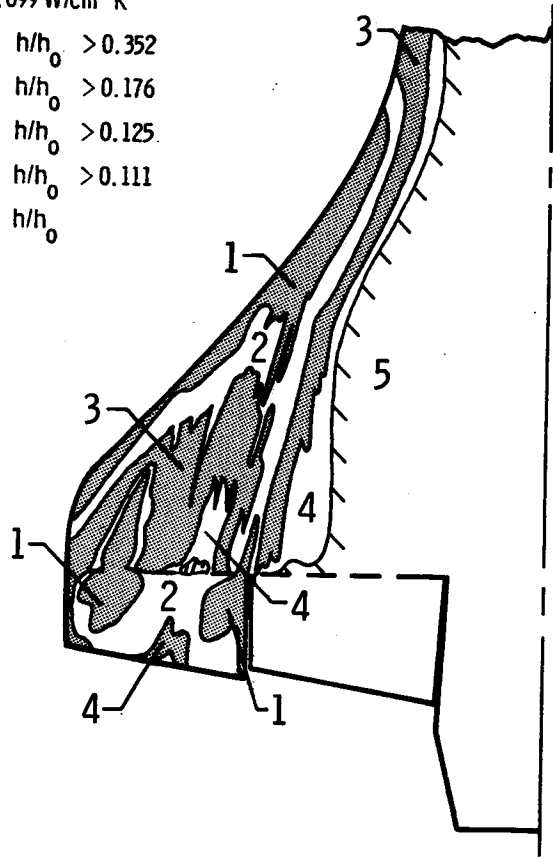
$N_{Re,L} = 4.29 \times 10^6$

$h_0 = 0.140 \, W/cm^2 K$

1          $h/h_0 > 0.832$

2 $0.832 > h/h_0 > 0.588$

3          $h/h_0 > 0.588$

4 $0.588 > h/h_0 > 0.480$

5 $0.480 > h/h_0 > 0.416$

6          $h/h_0 > 0.416$
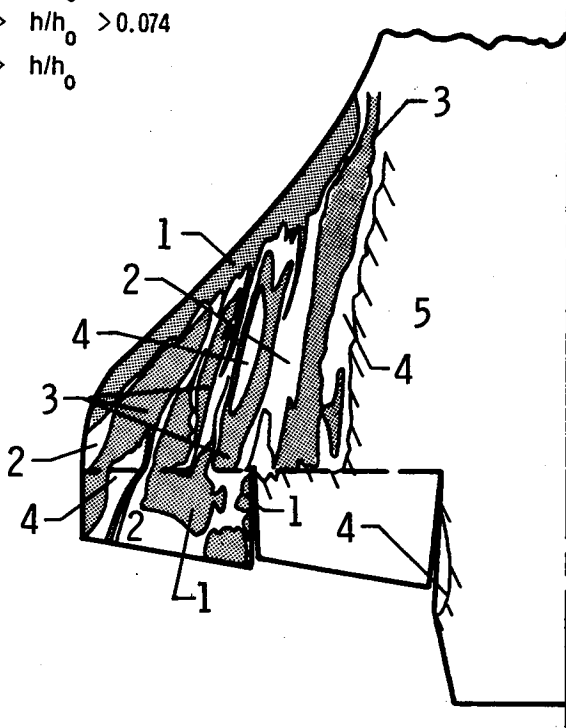
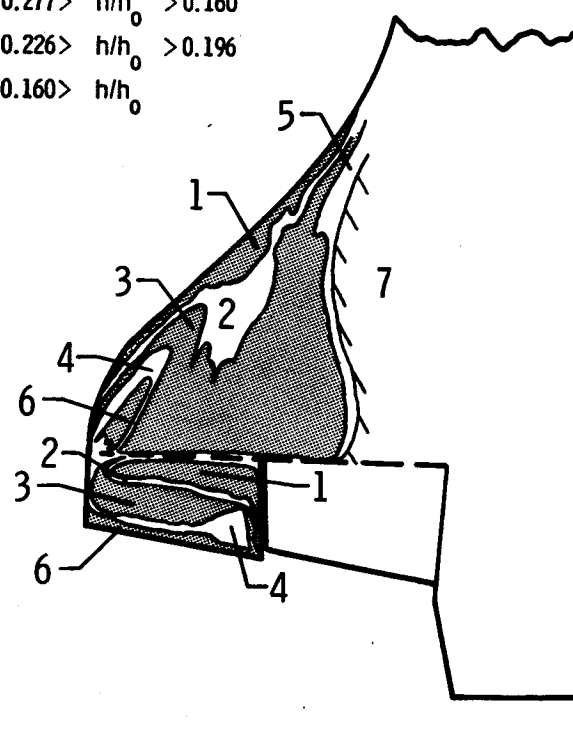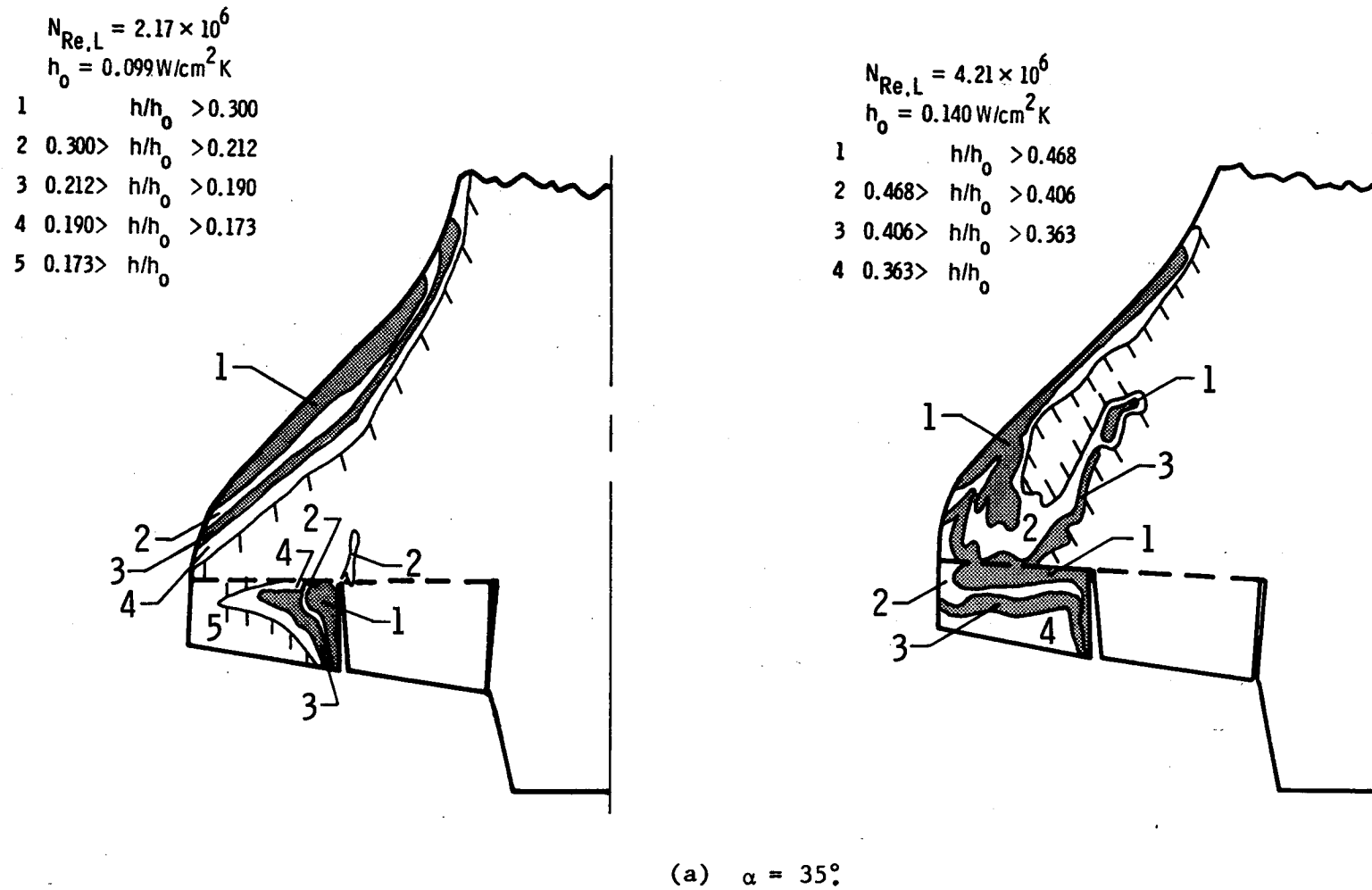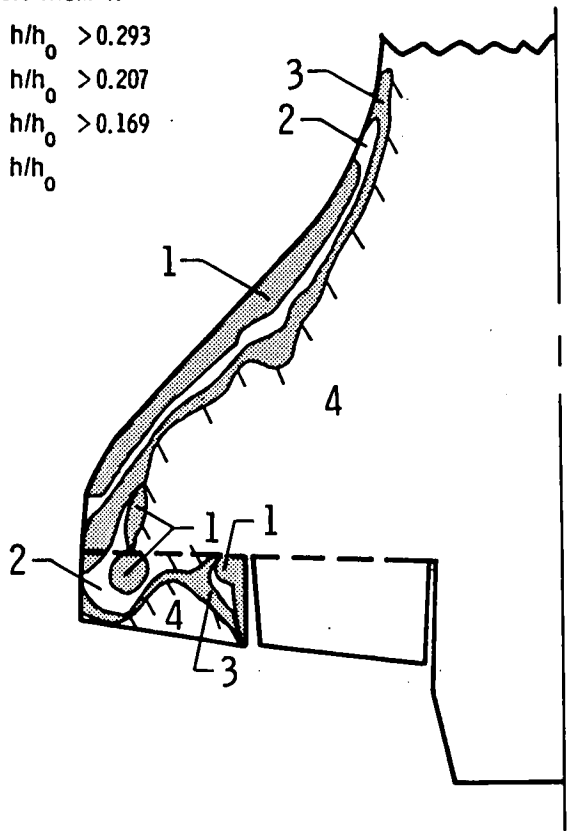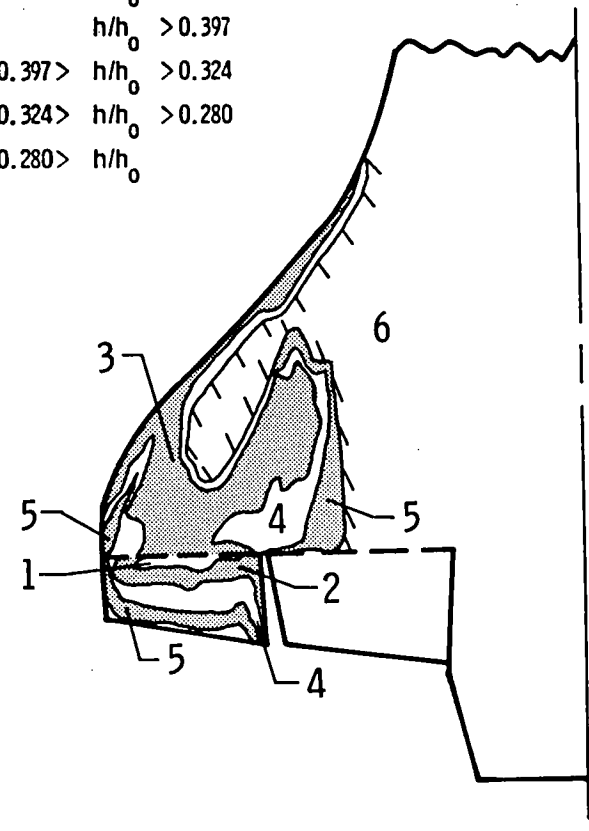7 $0.416 > h/h_0 > 0.294$

8 $0.294 > h/h_0$
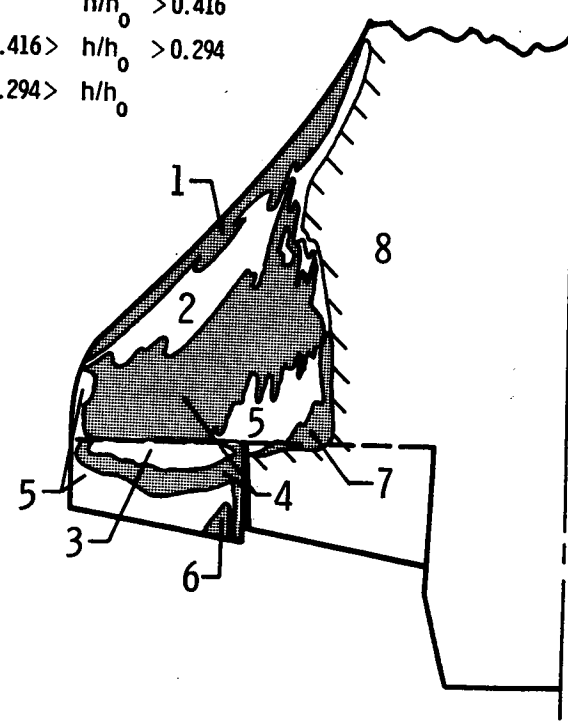
(b) $\alpha = 28°$.

Figure 5.- Continued.

$N_{Re,L} = 2.04 \times 10^6$
$h_0 = 0.099 \, \text{W/cm}^2\text{K}$

1   h/h_0 > 0.181
2   $0.181 >$ h/h_0 > 0.128
3   $0.128 >$ h/h_0 > 0.091
4   $0.191 >$ h/h_0 > 0.074
5   $0.074 >$ h/h_0

$N_{Re,L} = 4.21 \times 10^6$
$h_0 = 0.140 \, \text{W/cm}^2\text{K}$

1   h/h_0 > 0.554
2   $0.554 >$ h/h_0 > 0.392
3   $0.392 >$ h/h_0 > 0.277
4   $0.277 >$ h/h_0 > 0.226
5   $0.277 >$ h/h_0 > 0.160
6   $0.226 >$ h/h_0 > 0.196
7   $0.160 >$ h/h_0

(c) $\alpha = 20°$

Figure 5.- Concluded.

5(c)

$N_{Re,L} = 2.17 \times 10^6$

$h_0 = 0.099 \, W/cm^2 \, K$

1         $h/h_0 > 0.300$

2   $0.300 > h/h_0 > 0.212$

3   $0.212 > h/h_0 > 0.190$

4   $0.190 > h/h_0 > 0.173$

5   $0.173 > h/h_0$

$N_{Re,L} = 4.21 \times 10^6$

$h_0 = 0.140 \, W/cm^2 \, K$

1         $h/h_0 > 0.468$

2   $0.468 > h/h_0 > 0.406$

3   $0.406 > h/h_0 > 0.363$

4   $0.363 > h/h_0$

(a) $\alpha = 35°.$

Figure 6.- Heat-transfer coefficients and heating patterns on the orbiter wing and elevons at $\delta = 10$ and M = 6.

$N_{Re,L} = 2.09 \times 10^6$

$h_o = 0.097 \, W/cm^2 K$

1         $h/h_o \; > 0.293$

2   $0.293 > \; h/h_o \; > 0.207$

3   $0.207 > \; h/h_o \; > 0.169$

4   $0.169 > \; h/h_o$

$N_{Re,L} = 4.21 \times 10^6$

$h_o = 0.140 \, W/cm^2 K$

1         $h/h_o \; > 0.561$

2   $0.561 > \; h/h_o \; > 0.397$

3         $h/h_o \; > 0.397$

4   $0.397 > \; h/h_o \; > 0.324$

5   $0.324 > \; h/h_o \; > 0.280$

6   $0.280 > \; h/h_o$

(b) $\alpha = 28°$.

Figure 6.- Continued.

$N_{Re,L} = 2.09 \times 10^6$

$h_o = 0.099 \, W/cm^2 K$

1		h/h_o	> 0.450
2		h/h_o	> 0.260
3	$0.450 >$	h/h_o	> 0.201
4	$0.260 >$	h/h_o	> 0.142
5	$0.201 >$	h/h_o	> 0.142
6	$0.142 >$	h/h_o	

$N_{Re,L} = 4.21 \times 10^6$

$h_o = 0.140 \, W/cm^2 K$

1		h/h_o	> 0.406
2	$0.406 >$	h/h_o	> 0.274
3		h/h_o	> 0.274
4	$0.274 >$	h/h_o	> 0.203
5	$0.203 >$	h/h_o	> 0.182
6	$0.203 >$	h/h_o	
7	$0.182 >$	h/h_o	

(c) $\alpha = 20°$

Figure 6.- Concluded.

$N_{Re,L} = 2.17 \times 10^6$

$h_0 = 0.099 \ W/cm^2 K$

1		$h/h_0 > 1.126$
2	$1.126 >$	$h/h_0 > 0.975$
3	$0.975 >$	$h/h_0 > 0.872$
4	$0.872 >$	$h/h_0 > 0.689$
5	$0.689 >$	$h/h_0 > 0.563$
6	$0.563 >$	h/h_0
7		$h/h_0 > 0.465$
8	$0.465 >$	$h/h_0 > 0.329$
9	$0.329 >$	$h/h_0 > 0.269$
10	$0.269 >$	h/h_0

7

10

8

9

4 2

6

1

5 3
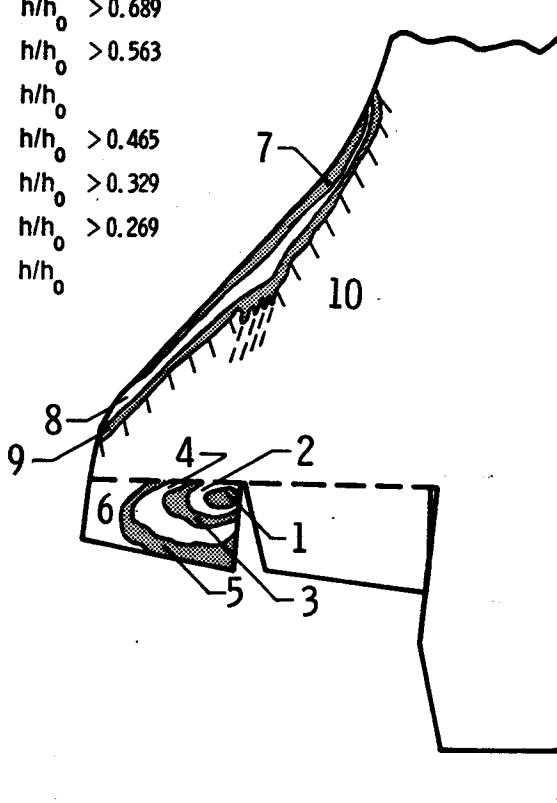
$N_{Re,L} = 4.44 \times 10^6$

$h_0 = 0.143 \ W/cm^2 K$

1		$h/h_0 > 2.197$
2	$2.197 >$	$h/h_0 > 1.794$
3	$1.794 >$	h/h_0

1

3 2
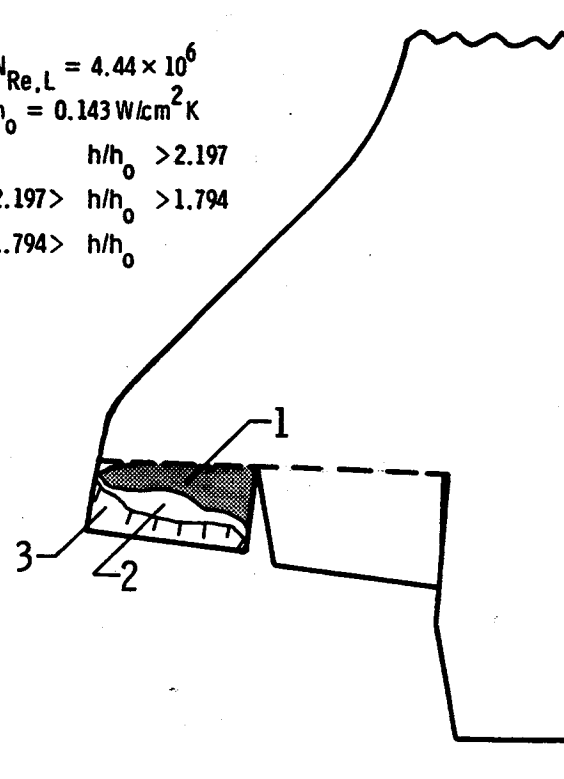
(a) $\alpha = 35°$

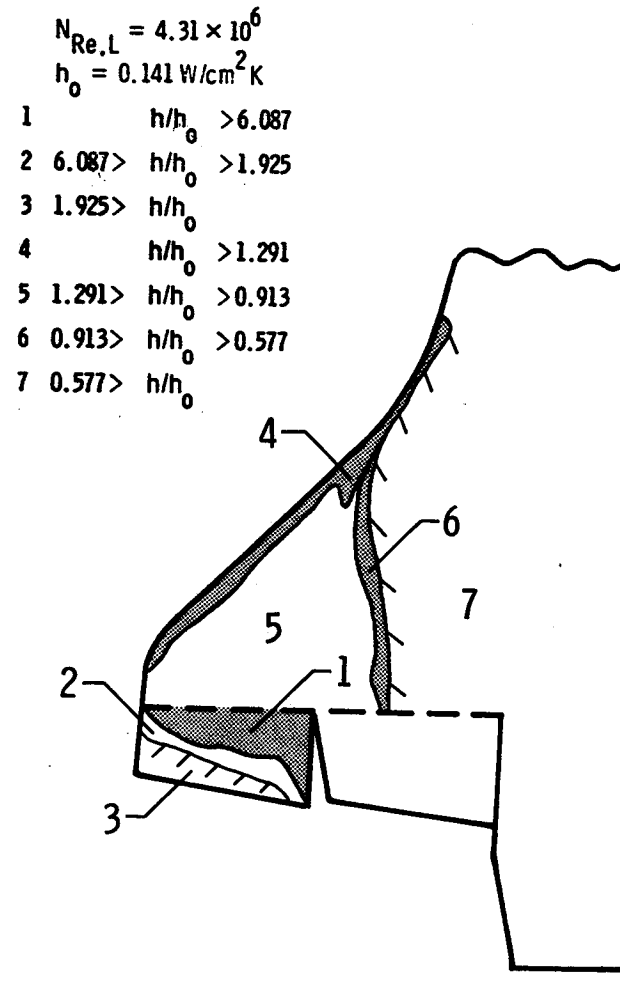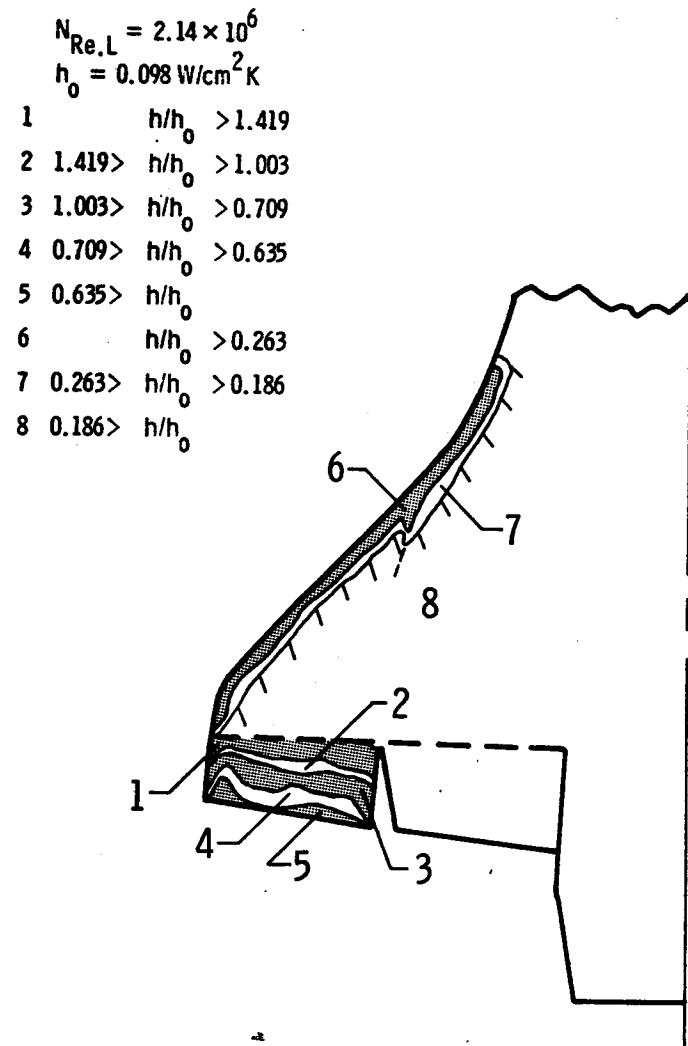Figure 7.- Heat-transfer coefficients and heating patterns on the orbiter wing and elevons at $\delta = 15$ and M = 6.

$N_{Re,L} = 2.14 \times 10^6$
$h_0 = 0.098 \, W/cm^2 K$

1		h/h_0	>1.419
2	$1.419>$	h/h_0	>1.003
3	$1.003>$	h/h_0	>0.709
4	$0.709>$	h/h_0	>0.635
5	$0.635>$	h/h_0	
6		h/h_0	>0.263
7	$0.263>$	h/h_0	>0.186
8	$0.186>$	h/h_0	

$N_{Re,L} = 4.31 \times 10^6$
$h_0 = 0.141 \, W/cm^2 K$

1		h/h_0	>6.087
2	$6.087>$	h/h_0	>1.925
3	$1.925>$	h/h_0	
4		h/h_0	>1.291
5	$1.291>$	h/h_0	>0.913
6	$0.913>$	h/h_0	>0.577
7	$0.577>$	h/h_0	

(b) $\alpha = 28°$

Figure 7.- Continued.

7(a)

$N_{Re,L} = 2.11 \times 10^6$

$h_0 = 0.098 \ W/cm^2 K$

1		h/h_0	> 0.347
2	$0.347 >$	h/h_0	> 0.325
3	$0.325 >$	h/h_0	> 0.265
4	$0.265 >$	h/h_0	
5		h/h_0	> 0.196
6	$0.196 >$	h/h_0	> 0.181
7	$0.181 >$	h/h_0	> 0.169
8	$0.169 >$	h/h_0	> 0.138
9	$0.138 >$	h/h_0	
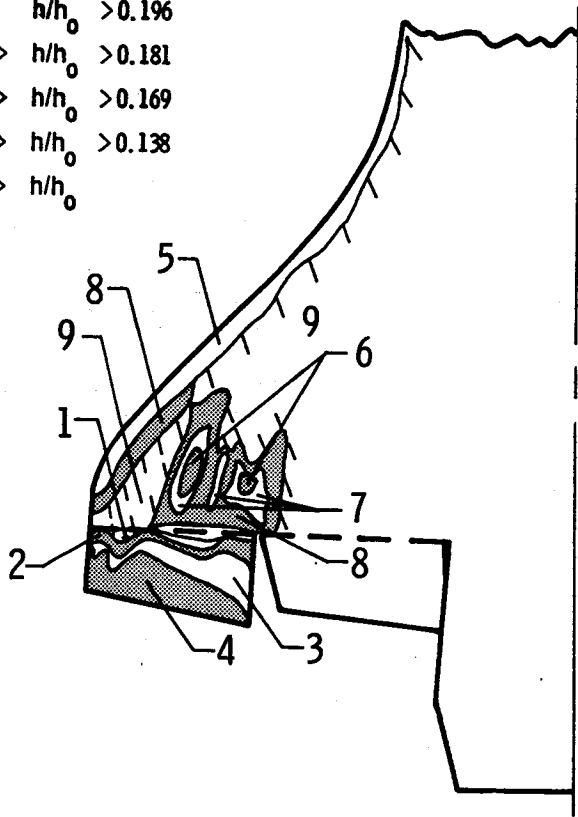
$N_{Re,L} = 4.32 \times 10^6$

$h_0 = 0.141 \ W/cm^2 K$

1		h/h_0	> 0.611
2	$0.611 >$	h/h_0	> 0.432
3		h/h_0	> 0.432
4	$0.432 >$	h/h_0	> 0.353
5	$0.353 >$	h/h_0	> 0.306
6	$0.306 >$	h/h_0	
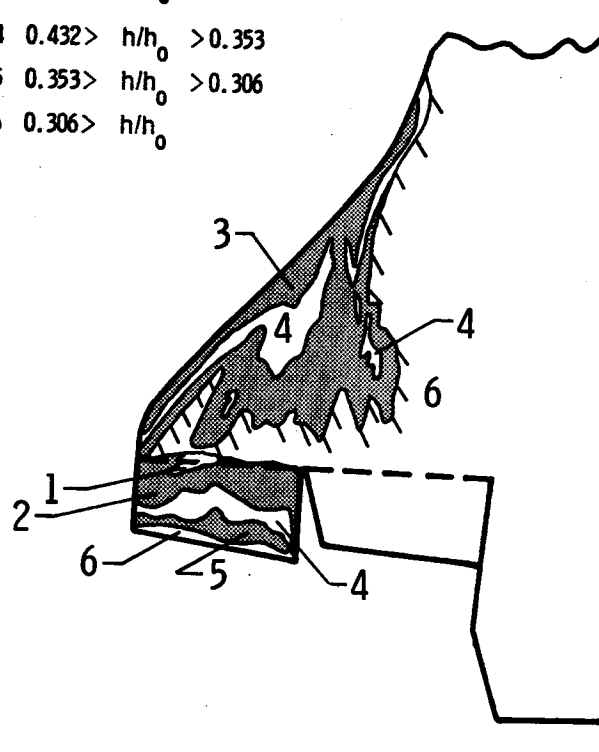
(c) $\alpha = 20°.$

Figure 7.- Concluded.

$N_{Re,L} = 2.11 \times 10^6$

$h_0 = 0.099 \, W/cm^2 K$

1		h/h_0	> 2.680
2	$2.680 >$	h/h_0	> 1.896
3	$1.896 >$	h/h_0	> 1.548
4	$1.548 >$	h/h_0	> 1.341
5	$1.341 >$	h/h_0	
6		h/h_0	> 0.290
7	$0.290 >$	h/h_0	> 0.237
8	$0.237 >$	h/h_0	> 0.205
9	$0.205 >$	h/h_0	> 0.175
10	$0.175 >$	h/h_0	
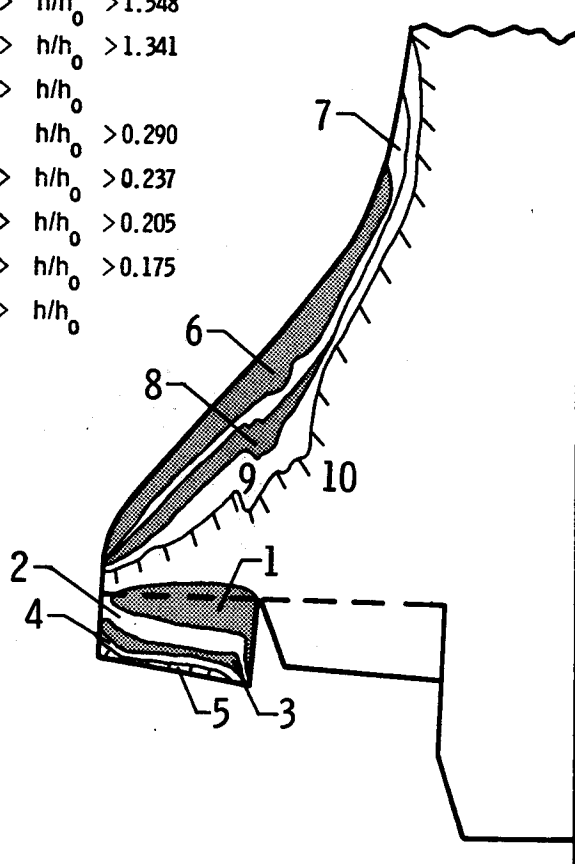
INSUFFICIENT
DATA

(a) $\alpha = 35°$

Figure 8.- Heat-transfer coefficients and heating patterns on the orbiter wing and elevons at $\delta = 20$ and M = 6.

8(a)

$N_{Re,L} = 2.07 \times 10^6$

$h_0 = 0.097 \ W/cm^2 K$

1		h/h_0	> 11.635
2	$11.635 >$	h/h_0	> 4.113
3	$4.113 >$	h/h_0	> 3.359
4	$3.359 >$	h/h_0	
5		h/h_0	> 0.318
6	$0.318 >$	h/h_0	> 0.223
7	$0.223 >$	h/h_0	> 0.184
8	$0.184 >$	h/h_0	
9	$0.223 >$	h/h_0	
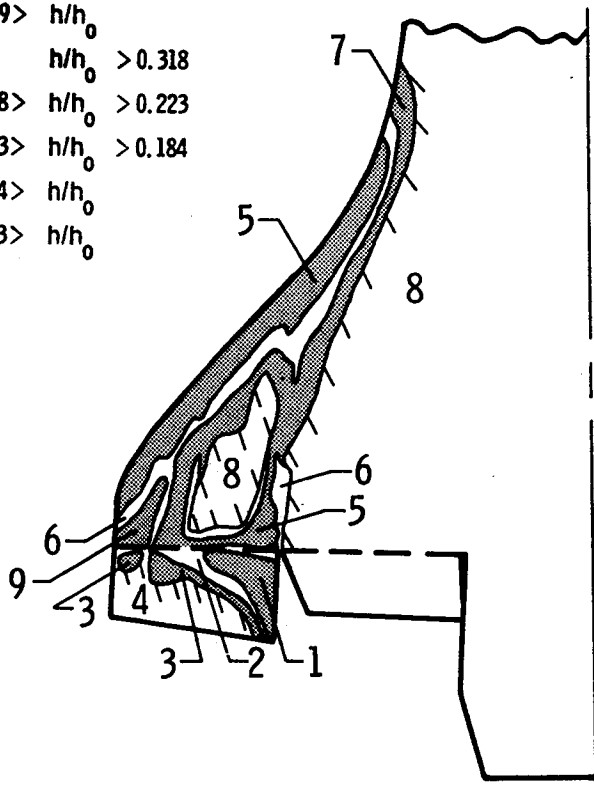
INSUFFICIENT
DATA

(b) $\alpha = 28°$.

Figure 8.- Continued.

$N_{Re,L} = 4.28 \times 10^6$

$h_o = 0.141 \, W/cm^2 K$

1		h/h_o	>1.728
2	$1.728>$	h/h_o	>1.222
3	$1.222>$	h/h_o	>0.864
4	$0.864>$	h/h_o	>0.706
5		h/h_o	>0.593
6	$0.593>$	h/h_o	>0.419
7	$0.419>$	h/h_o	>0.342
8	$0.342>$	h/h_o	>0.296
9	$0.296>$	h/h_o	

INSUFFICIENT
DATA
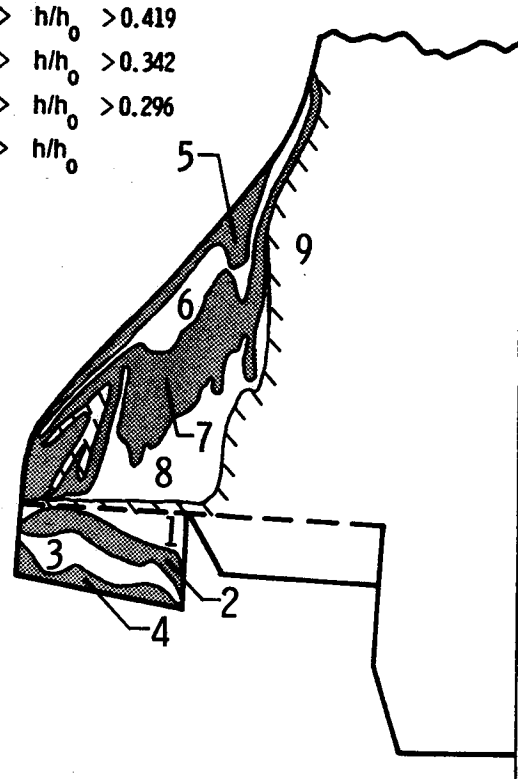
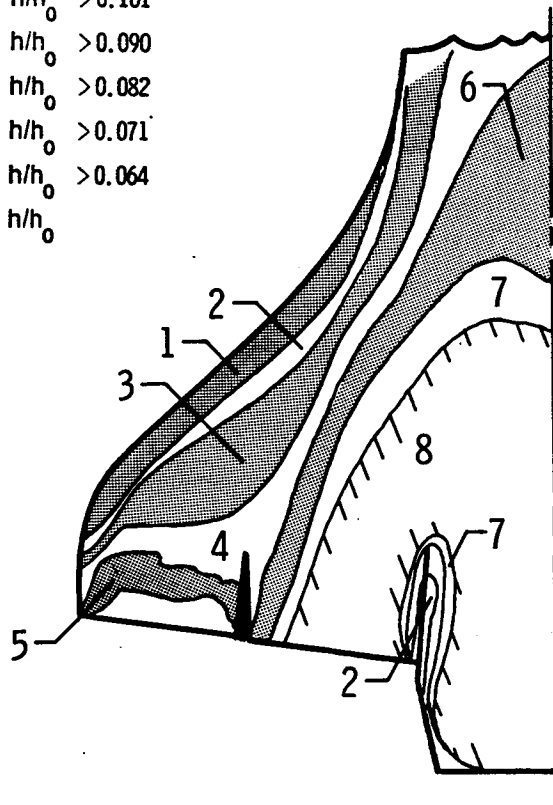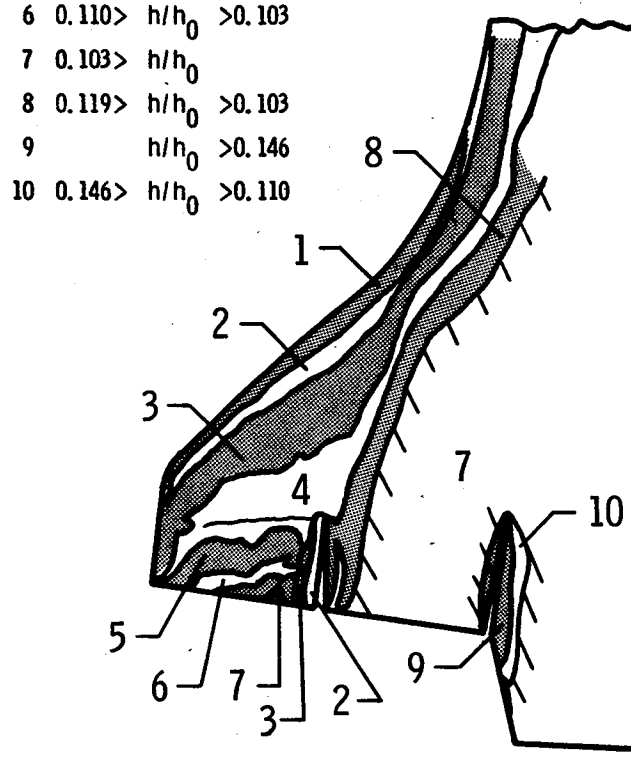(c) $\alpha = 20°$

Figure 8.- Concluded.

8(c)

$N_{Re,L} = 0.52 \times 10^6$

$h_0 = 0.059 \, W/cm^2 K$

1   h/h_0 >0.202

2   0.202> h/h_0 >0.143

3   0.143> h/h_0 >0.101

4   0.101> h/h_0 >0.090

5   0.090>. h/h_0 >0.082

6   0.082> h/h_0 >0.071

7   0.071> h/h_0 >0.064

8   0.064> h/h_0

$N_{Re,L} = 2.10 \times 10^6$

$h_0 = 0.114 \, W/cm^2 K$

1   h/h_0 >0.291

2   0.291> h/h_0 >0.206

3   0.206> h/h_0 >0.146

4   0.146> h/h_0 >0.119

5   0.119> h/h_0 >0.110

6   0.110> h/h_0 >0.103

7   0.103> h/h_0

8   0.119> h/h_0 >0.103

9   h/h_0 >0.146

10   0.146> h/h_0 >0.110
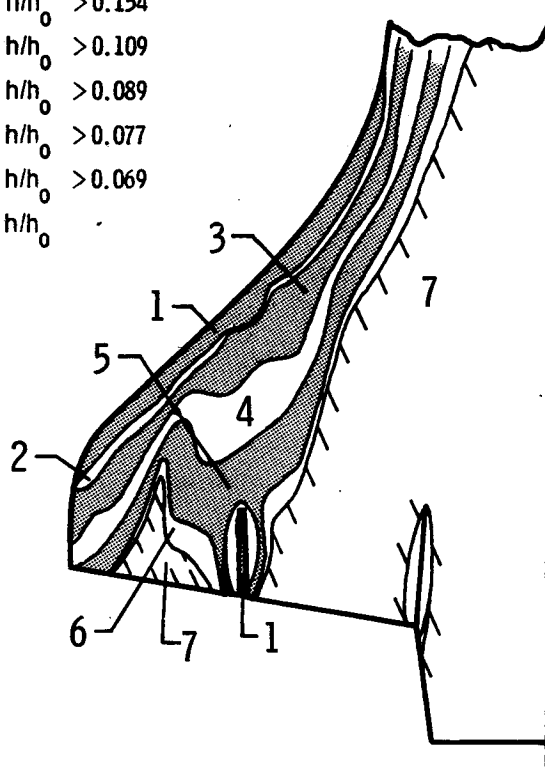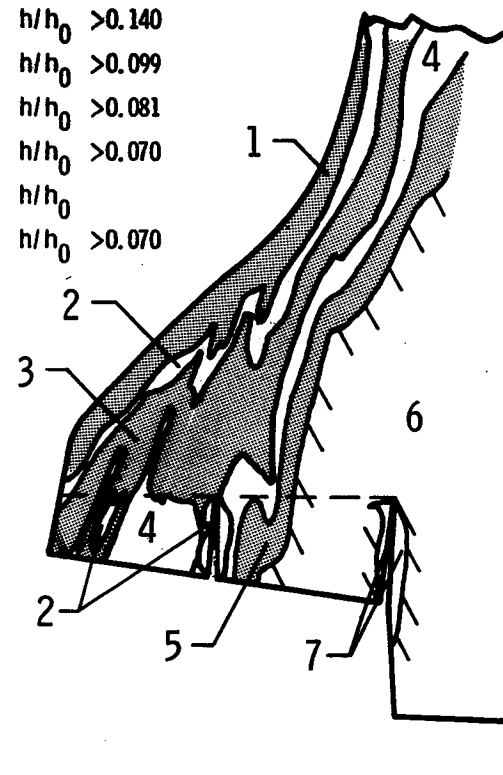
(a) $\alpha = 35°$

Figure 9.– Heat–transfer coefficients and heating patterns on the orbiter wing and elevons at $\delta = 0$ and M = 10.

$N_{Re,L} = 0.52 \times 10^6$
$h_o = 0.059 \, W/cm^2 K$

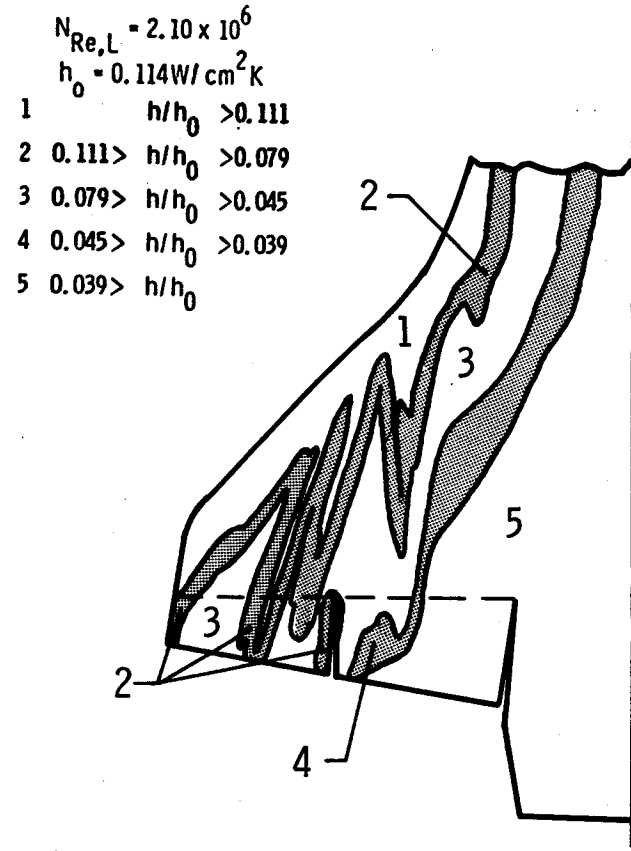|		
1		$h/h_o > 0.218$
2	$0.218 >$	$h/h_o > 0.154$
3	$0.154 >$	$h/h_o > 0.109$
4	$0.109 >$	$h/h_o > 0.089$
5	$0.089 >$	$h/h_o > 0.077$
6	$0.077 >$	$h/h_o > 0.069$
7	$0.069 >$	h/h_o

$N_{Re,L} = 2.10 \times 10^6$
$h_o = 0.114 \, W/cm^2 K$

1		$h/h_o > 0.198$
2	$0.198 >$	$h/h_o > 0.140$
3	$0.140 >$	$h/h_o > 0.099$
4	$0.099 >$	$h/h_o > 0.081$
5	$0.081 >$	$h/h_o > 0.070$
6	$0.070 >$	h/h_o
7		$h/h_o > 0.070$

(b) $\alpha = 28°$

Figure 9.- Continued.

9(h)

$N_{Re,L} = 0.52 \times 10^6$
$h_0 = 0.059 \, W/cm^2 K$

1   h/h_0 >0.129

2   $0.129>$ h/h_0 >0.091

3   $0.091>$ h/h_0 >0.064

4   $0.064>$ h/h_0 >0.045

5   $0.045>$ h/h_0

$N_{Re,L} = 2.10 \times 10^6$
$h_0 = 0.114 \, W/cm^2 K$

1   h/h_0 >0.111

2   $0.111>$ h/h_0 >0.079

3   $0.079>$ h/h_0 >0.045

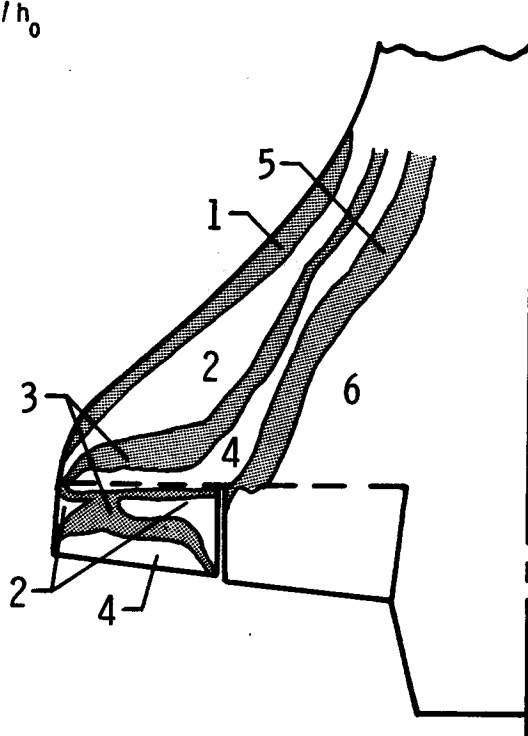4 $0.045>$ h/h_0 >0.039

5   $0.039>$ h/h_0

(c) $\alpha = 20°$

Figure 9.- Concluded.

9(c)

$N_{Re,L} = 0.52 \times 10^6$
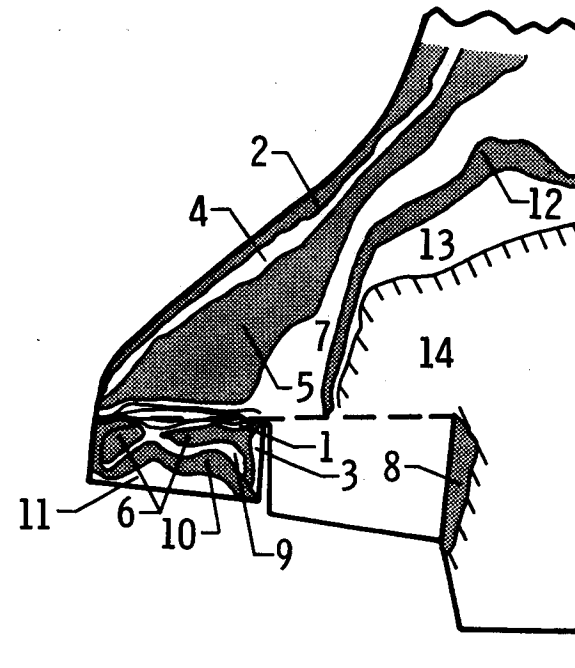
$h_0 = 0.059 W/cm^2 K$

1      $h/h_0 > 0.253$

2   $0.253 > h/h_0 > 0.127$

3   $0.127 > h/h_0 > 0.113$

4   $0.113 > h/h_0 > 0.096$

5   $0.096 > h/h_0 > 0.080$

6   $0.080 > h/h_0$

$N_{Re,L} = 2.10 \times 10^6$

$h_0 = 0.114 W/cm^2 K$

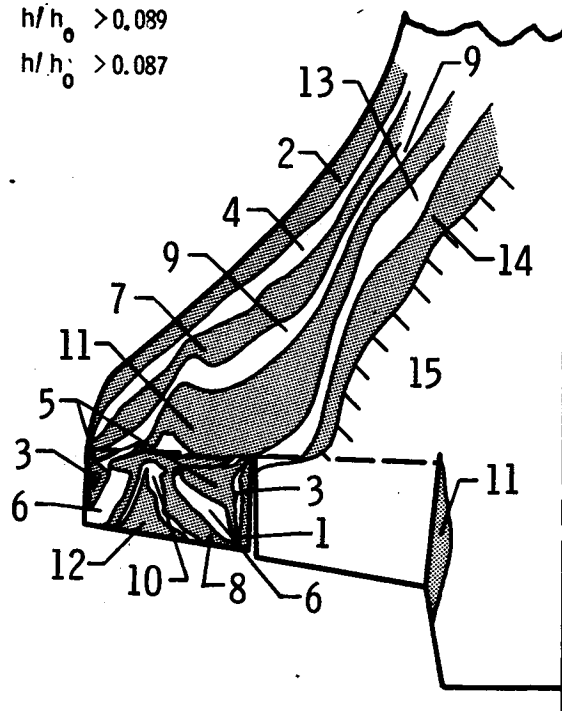|					
1		$h/h_0 > 0.348$	8		$h/h_0 > 0.101$
2		$h/h_0 > 0.268$	9	$0.132 >$	$h/h_0 > 0.123$
3	$0.348 >$	$h/h_0 > 0.174$	10	$0.123 >$	$h/h_0 > 0.110$
4	$0.268 >$	$h/h_0 > 0.190$	11	$0.110 >$	h/h_0
5	$0.190 >$	$h/h_0 > 0.134$	12	$0.101 >$	$h/h_0 > 0.095$
6	$0.174 >$	$h/h_0 > 0.132$	13	$0.095 >$	$h/h_0 > 0.085$
7	$0.134 >$	$h/h_0 > 0.101$	14	$0.085 >$	h/h_0

(a) $\alpha = 35°$

Figure 10.— Heat-transfer coefficients and heating patterns on the orbiter wing and elevons at $\delta = 5$ and $M = 10$.

10(a)
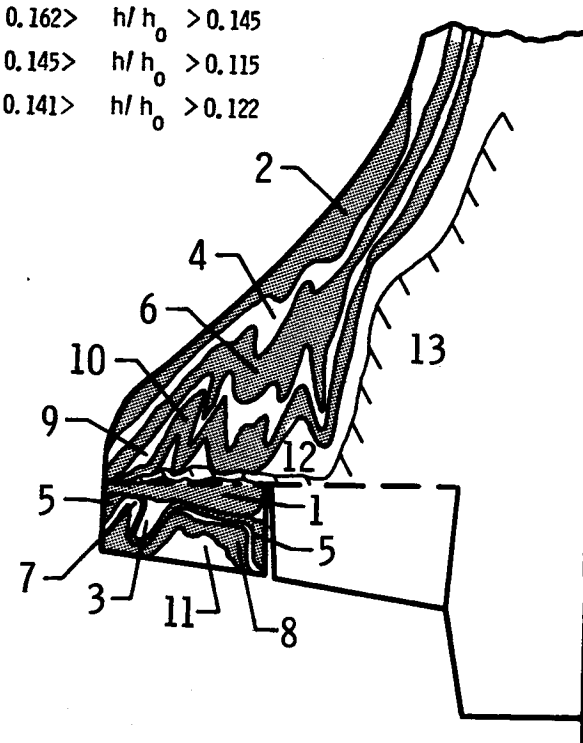
$N_{Re,L} = 0.52 \times 10^6$
$h_o = 0.059 \, W/cm^2 K$

1	$h/h_o > 0.177$		10	$0.089 > h/h_o > 0.087$	
2	$h/h_o > 0.173$		11	$0.087 > h/h_o > 0.079$	
3	$0.177 > h/h_o > 0.145$		12	$0.079 > h/h_o > 0.071$	
4	$0.173 > h/h_o > 0.123$		13	$0.071 > h/h_o$	
5	$0.145 > h/h_o > 0.125$		14	$0.061 > h/h_o > 0.061$	
6	$0.125 > h/h_o > 0.102$		15	$0.055 > h/h_o > 0.055$	
7	$0.123 > h/h_o > 0.100$				
8	$0.102 > h/h_o > 0.089$				
9	$0.100 > h/h_o > 0.087$				

$N_{Re,L} = 2.10 \times 10^6$
$h_o = 0.114 \, W/cm^2 K$

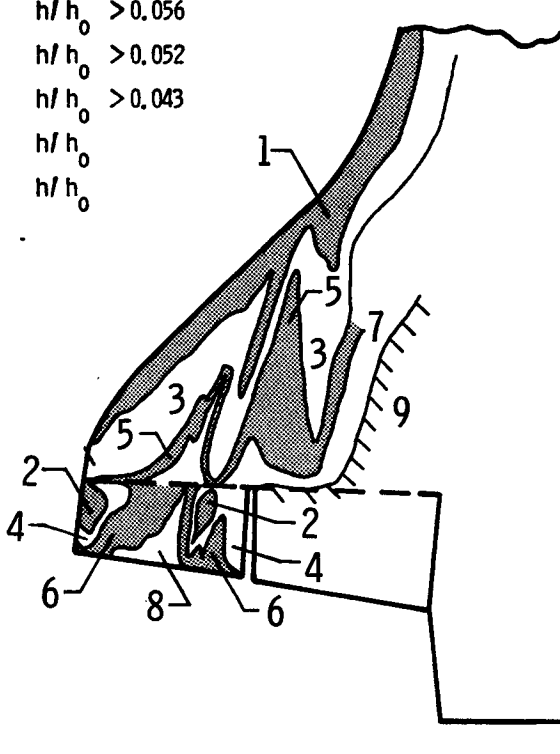|				
1	$h/h_o > 0.324$	10	$0.122 > h/h_o > 0.109$
2	$h/h_o > 0.244$	11	$0.115 > h/h_o$
3	$0.324 > h/h_o > 0.187$	12	$0.109 > h/h_o > 0.086$
4	$0.244 > h/h_o > 0.172$	13	$0.086 > h/h_o$
5	$0.187 > h/h_o > 0.162$		
6	$0.172 > h/h_o > 0.141$		
7	$0.162 > h/h_o > 0.145$		
8	$0.145 > h/h_o > 0.115$		
9	$0.141 > h/h_o > 0.122$		

(b) $\alpha = 28°$

Figure 10.- Continued.

$N_{Re,L} = 0.52 \times 10^6$
$h_o = 0.059 \, W/cm^2 K$

1		$h/h_o > 0.137$
2		$h/h_o > 0.083$
3	$0.137 >$	$h/h_o > 0.069$
4	$0.083 >$	$h/h_o > 0.068$
5	$0.069 >$	$h/h_o > 0.056$
6	$0.068 >$	$h/h_o > 0.052$
7	$0.056 >$	$h/h_o > 0.043$
8	$0.052 >$	h/h_o
9	$0.043 >$	h/h_o

$N_{Re,L} = 2.10 \times 10^6$
$h_o = 0.114 \, W/cm^2 K$

1		$h/h_o > 0.237$
2		$h/h_o > 0.184$
3	$0.237 >$	$h/h_o > 0.118$
4	$0.184 >$	$h/h_o > 0.092$
5	$0.118 >$	$h/h_o > 0.084$
6	$0.091 >$	$h/h_o > 0.065$
7	$0.084 >$	h/h_o
8	$0.065 >$	h/h_o
9	$0.065 >$	
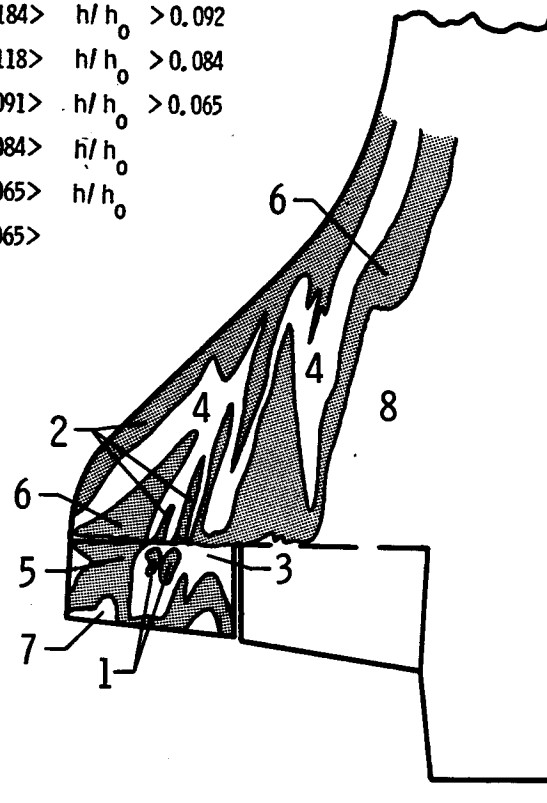
(c) $\alpha = 20°$

Figure 10.- Concluded.

$10(c)$

INSUFFICIENT
DATA

$N_{Re,L} = 2.10 \times 10^6$

$h_0 = 0.114 W/cm^2 K$

1	$h/h_0 > 0.309$
2	$0.309 > h/h_0 > 0.219$
3	$0.309 > h/h_0 > 0.109$
4	$0.219 > h/h_0 > 0.155$
5	$h/h_0 > 0.180$
6	$0.180 > h/h_0 > 0.127$
7	$0.155 > h/h_0 > 0.109$
8	$0.127 > h/h_0 > 0.114$
9	$0.114 > h/h_0$
10	$0.109 > h/h_0 > 0.098$
11	$0.098 > h/h_0$
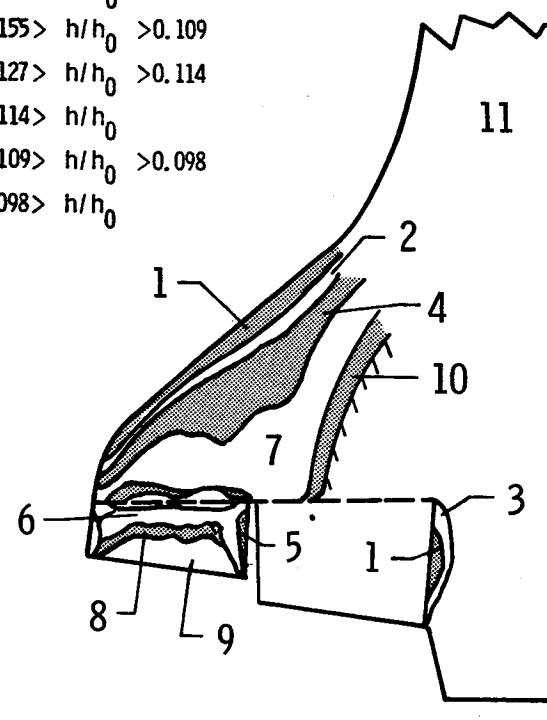
(a) $\alpha = 35°$

Figure 11.- Heat-transfer coefficients and heating patterns on the orbiter wing and elevons at $\delta = 10$ and $M = 10$.

11 (a)

$N_{Re,L} = 0.52 \times 10^6$
$h_0 = 0.059$ W/cm²K

1		h/h_0	>0.179	9	$0.080>$	h/h_0	
2	$0.179>$	h/h_0	>0.126	10	$0.073>$	h/h_0	>0.063
3		h/h_0	>0.126	11	$0.063>$	h/h_0	>0.057
4	$0.126>$	h/h_0	>0.103	12	$0.057>$	h/h_0	
5	$0.126>$	h/h_0	>0.089				
6	$0.103>$	h/h_0	>0.089				
7	$0.089>$	h/h_0	>0.080				
8	$0.089>$	h/h_0	>0.073				

$N_{Re,L} = 2.10 \times 10^6$
$h_0 = 0.114$ W/cm²K

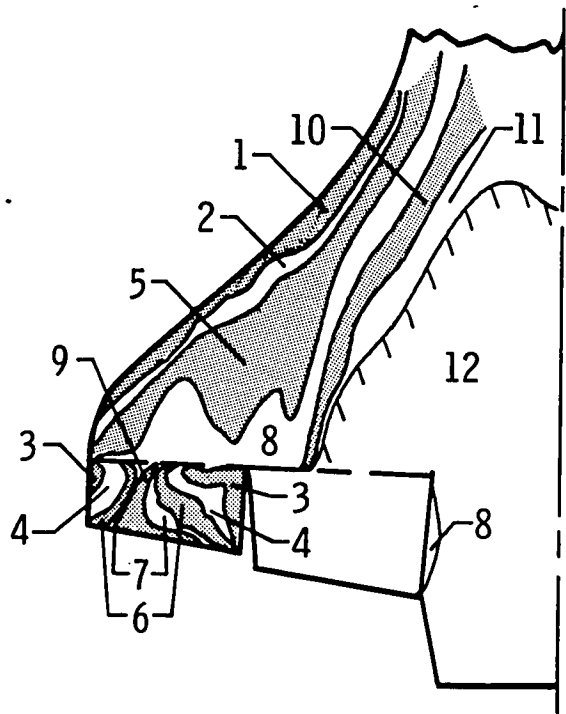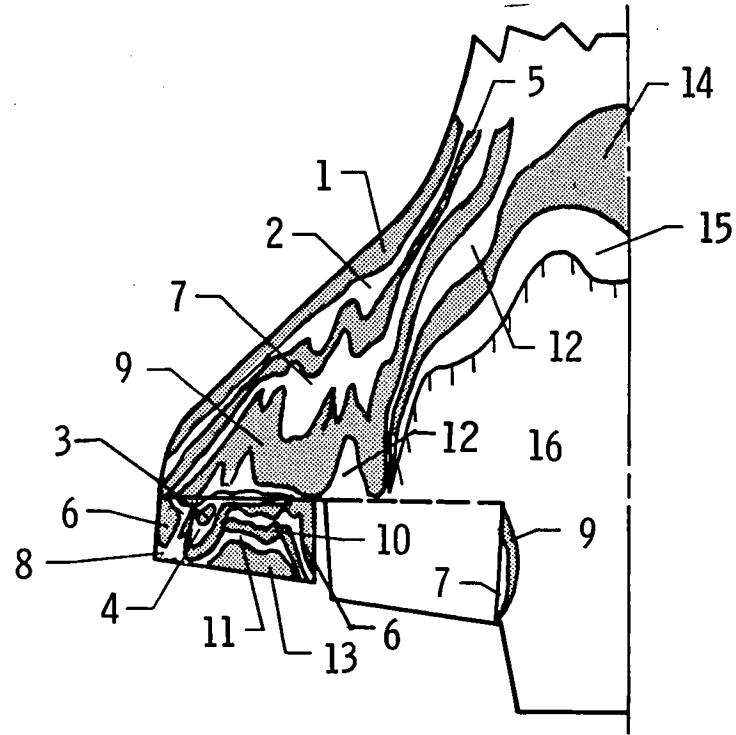| 1		h/h_0	>0.242	9	$0.121>$	h/h_0	>0.099
2	$0.242>$	h/h_0	>0.171	10	$0.114>$	h/h_0	>0.102
3		h/h_0	>0.186	11	$0.102>$	h/h_0	>0.093
4	$0.186>$	h/h_0	>0.161	12	$0.099>$	h/h_0	>0.085
5	$0.171>$	h/h_0	>0.140	13	$0.093>$	h/h_0	
6	$0.161>$	h/h_0	>0.131	14	$0.085>$	h/h_0	>0.076
7	$0.140>$	h/h_0	>0.121	15	$0.076>$	h/h_0	>0.070
8	$0.131>$	h/h_0	>0.114	16	$0.070>$	h/h_0	

(b) $\alpha = 28°$

Figure 11.- Continued.

$N_{Re,L} = 0.52 \times 10^6$
$h_0 = 0.059 \, W/cm^2 K$

1		h/h_0	>0.144	11	$0.059>$	h/h_0	>0.051
2	$0.144>$	h/h_0	>0.102	12	$0.051>$	h/h_0	>0.046
3		h/h_0	>0.114	13	$0.046>$	h/h_0	>0.042
4	$0.114>$	h/h_0	>0.093	14	$0.042>$	h/h_0	
5	$0.102>$	h/h_0	>0.072				
6	$0.093>$	h/h_0	>0.081				
7	$0.081>$	h/h_0	>0.072				
8	$0.072>$	h/h_0	>0.066				
9	$0.066>$	h/h_0					
10	$0.072>$	h/h_0	>0.059				

$N_{Re,L} = 2.10 \times 10^6$
$h_0 = 0.114 \, W/cm^2 K$

1		h/h_0	>0.198
2	$0.198>$	h/h_0	>0.140
3	$0.140>$	h/h_0	>0.114
4		h/h_0	>0.117
5	$0.117>$	h/h_0	>0.083
6	$0.114>$	h/h_0	>0.099
7	$0.099>$	h/h_0	
8	$0.083>$	h/h_0	>0.068
9	$0.068>$	h/h_0	>0.059
10	$0.059>$	h/h_0	

(c) $\alpha = 20°$

Figure 11.- Concluded.

11(c)

$N_{Re,L} = 0.52 \times 10^6$

$h_0 = 0.059 \, W/cm^2 K$

1		h/h_0	> 0.451
2	$0.451 >$	h/h_0	> 0.260
3		h/h_0	> 0.261
4	$0.261 >$	h/h_0	> 0.184
5	$0.260 >$	h/h_0	> 0.225
6	$0.225 >$	h/h_0	> 0.202
7	$0.202 >$	h/h_0	
8	$0.184 >$	h/h_0	> 0.130
9	$0.130 >$	h/h_0	> 0.107
10	$0.107 >$	h/h_0	> 0.092
11	$0.092 >$	h/h_0	> 0.083
12	$0.083 >$	h/h_0	

$N_{Re,L} = 2.10 \times 10^6$

$h_0 = 0.114 \, W/cm^2 K$

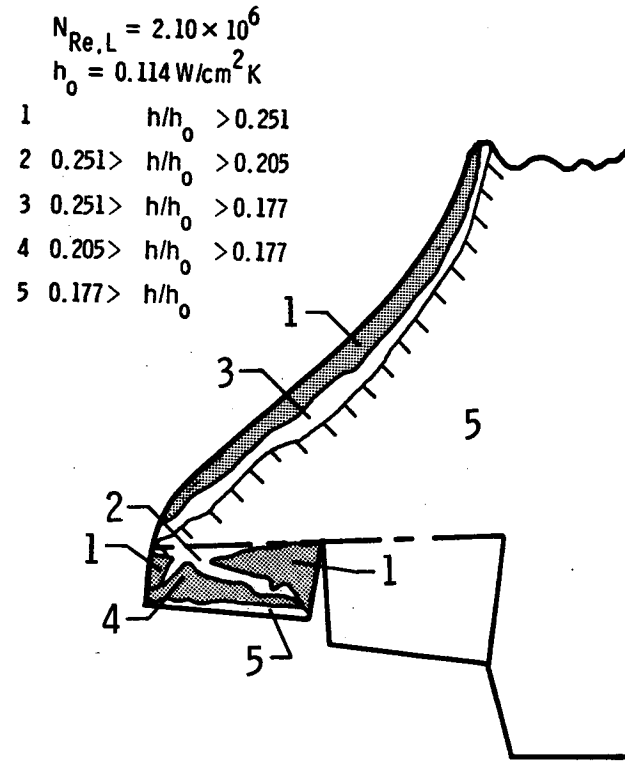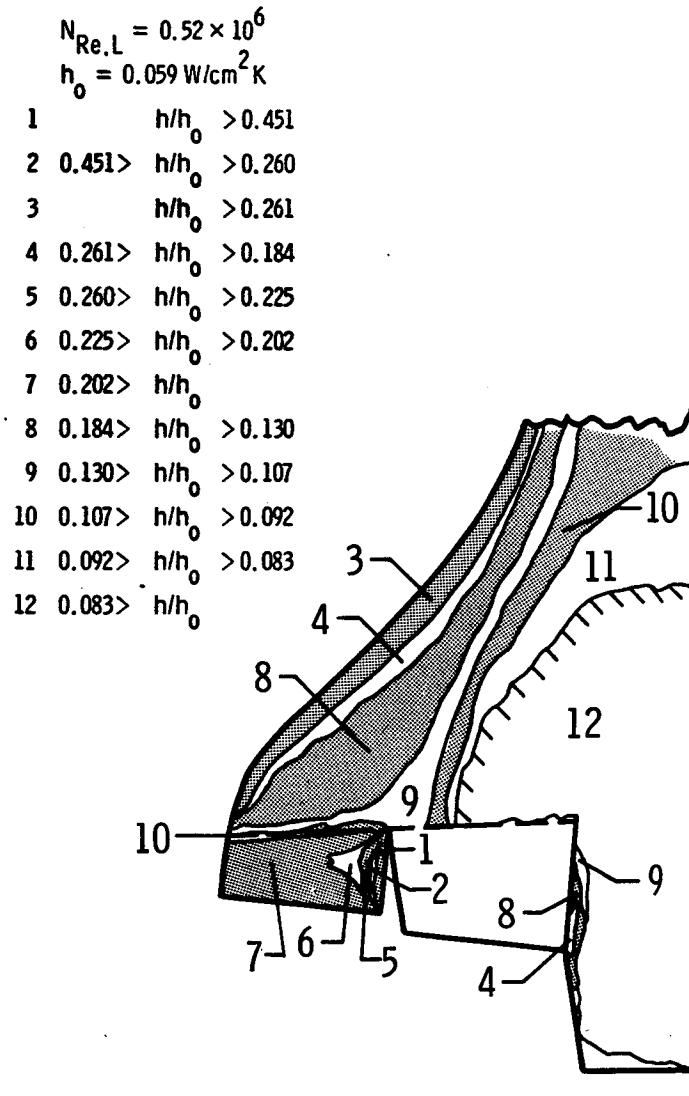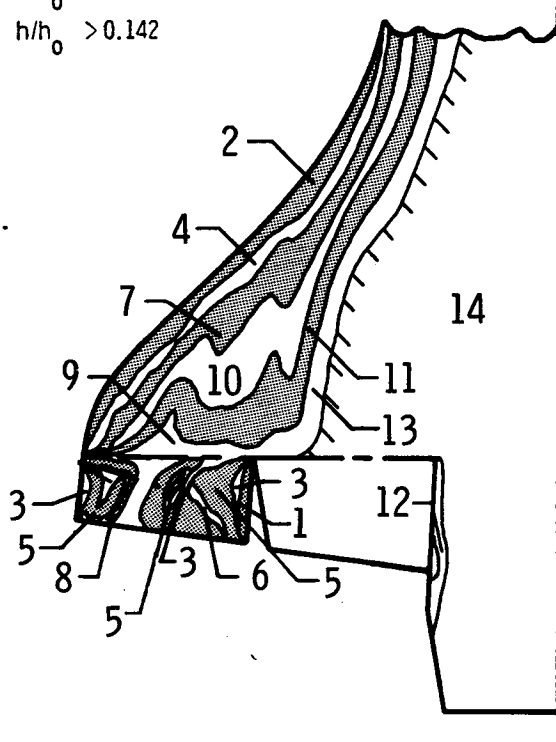| 1		h/h_0	> 0.251
2	$0.251 >$	h/h_0	> 0.205
3	$0.251 >$	h/h_0	> 0.177
4	$0.205 >$	h/h_0	> 0.177
5	$0.177 >$	h/h_0	

(a) $\alpha = 35°$

Figure 12.– Heat-transfer coefficients and heating patterns on the orbiter wing and elevons at $\delta = 15$ and $M = 10$.

$$N_{Re,L} = 0.52 \times 10^6$$
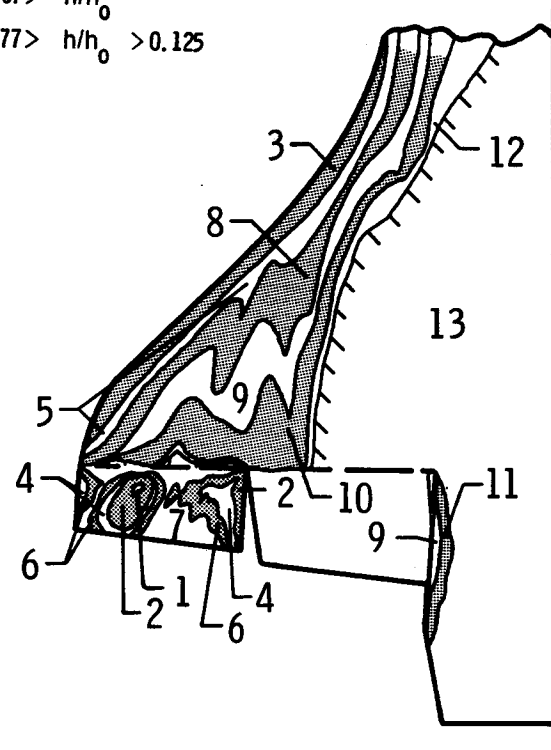$$h_0 = 0.059 \ \text{W/cm}^2\text{K}$$

1		h/h_0	> 0.333
2		h/h_0	> 0.254
3	$0.333 >$	h/h_0	> 0.235
4	$0.254 >$	h/h_0	> 0.180
5	$0.235 >$	h/h_0	> 0.192
6	$0.192 >$	h/h_0	> 0.166
7	$0.180 >$	h/h_0	> 0.127
8	$0.166 >$	h/h_0	> 0.142
9	$0.142 >$	h/h_0	
10	$0.127 >$	h/h_0	> 0.104
11	$0.104 >$	h/h_0	> 0.090
12	$0.104 >$	h/h_0	> 0.077
13	$0.090 >$	h/h_0	> 0.077
14	$0.077 >$	h/h_0	

$$N_{Re,L} = 2.10 \times 10^6$$
$$h_0 = 0.114 \ \text{W/cm}^2\text{K}$$

1		h/h_0	> 0.463
2	$0.463 >$	h/h_0	> 0.327
3		h/h_0	> 0.251
4	$0.327 >$	h/h_0	> 0.231
5	$0.251 >$	h/h_0	> 0.177
6	$0.231 >$	h/h_0	> 0.207
7	$0.207 >$	h/h_0	
8	$0.177 >$	h/h_0	> 0.125
9	$0.125 >$	h/h_0	> 0.102
10	$0.102 >$	h/h_0	> 0.089
11	$0.102 >$	h/h_0	> 0.079
12	$0.089 >$	h/h_0	> 0.079
13	$0.079 >$	h/h_0	

(b) $\alpha = 28°$.

Figure 12.- Continued.

$N_{Re,L} = 0.52 \times 10^6$
$h_0 = 0.059 \, W/cm^2 K$

1		h/h_0	> 0.348
2	$0.348 >$	h/h_0	> 0.246
3	$0.246 >$	h/h_0	> 0.201
4	$0.201 >$	h/h_0	> 0.174
5	$0.174 >$	h/h_0	
6		h/h_0	> 0.169
7	$0.169 >$	h/h_0	> 0.120
8	$0.120 >$	h/h_0	> 0.085
9	$0.085 >$	h/h_0	> 0.069
10	$0.069 >$	h/h_0	> 0.060
11	$0.060 >$	h/h_0	> 0.054
12	$0.054 >$	h/h_0	
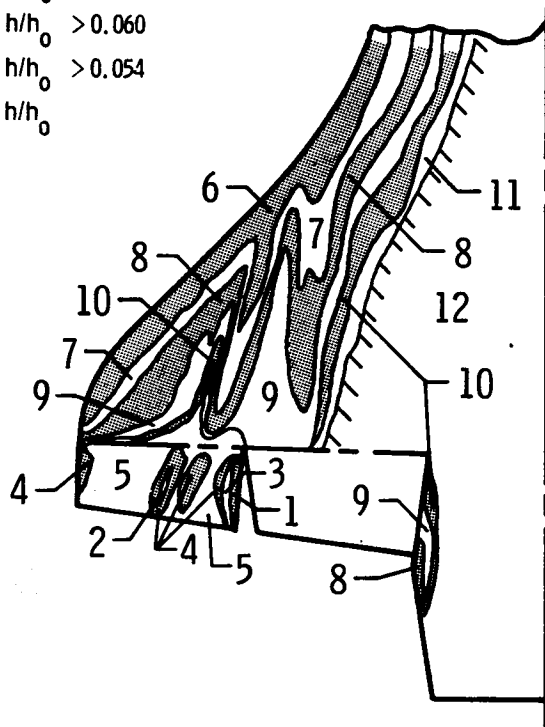
$N_{Re,L} = 2.10 \times 10^6$
$h_0 = 0.114 \, W/cm^2 K$

1		h/h_0	> 0.418
2	$0.418 >$	h/h_0	> 0.295
3	$0.295 >$	h/h_0	> 0.241
4	$0.241 >$	h/h_0	> 0.171
5	$0.171 >$	h/h_0	> 0.132
6	$0.132 >$	h/h_0	
7		h/h_0	> 0.127
8	$0.127 >$	h/h_0	> 0.090
9	$0.090 >$	h/h_0	> 0.073
10	$0.073 >$	h/h_0	> 0.052
11	$0.052 >$	h/h_0	> 0.040
12	$0.040 >$	h/h_0	

(c) $\alpha = 20°$.

Figure 12.- Concluded.

$N_{Re,L} = 0.52 \times 10^6$
$h_0 = 0.059 \, W/cm^2 K$

1		h/h_0	>0.632
2	$0.632>$	h/h_0	>0.316
3	$0.316>$	h/h_0	>0.258
4	$0.258>$	h/h_0	>0.224
5		h/h_0	>0.237
6	$0.237>$	h/h_0	>0.167
7	$0.224>$	h/h_0	>0.191
8	$0.191>$	h/h_0	
9	$0.167>$	h/h_0	>0.118
10	$0.118>$	h/h_0	>0.097
11	$0.097>$	h/h_0	>0.084
12	$0.084>$	h/h_0	>0.071
13	$0.071>$	h/h_0	

$N_{Re,L} = 2.10 \times 10^6$
$h_0 = 0.114 \, W/cm^2 K$

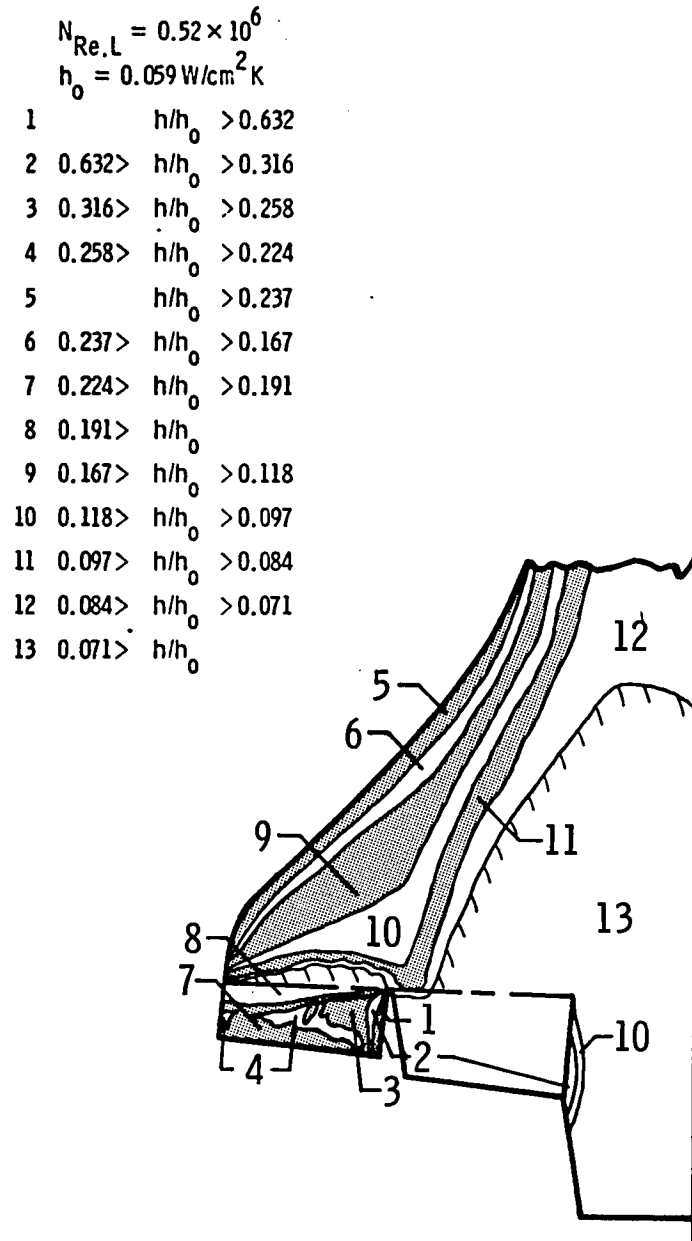| 1		h/h_0	>0.585
2	$0.585>$	h/h_0	>0.478
3	$0.478>$	h/h_0	>0.414
4	$0.414>$	h/h_0	>0.370
5	$0.370>$	h/h_0	
6		h/h_0	>0.259
7	$0.259>$	h/h_0	>0.183
8	$0.183>$	h/h_0	>0.150
9	$0.150>$	h/h_0	>0.130
10	$0.130>$	h/h_0	>0.116
11	$0.116>$	h/h_0	>0.092
12	$0.092>$	h/h_0	>0.082
13	$0.082>$	h/h_0	

(a) $\alpha = 35°$.

Figure 13.- Heat-transfer coefficients and heating patterns on the orbiter wing and elevons at $\delta = 20$ and $M = 10$.

13(a)
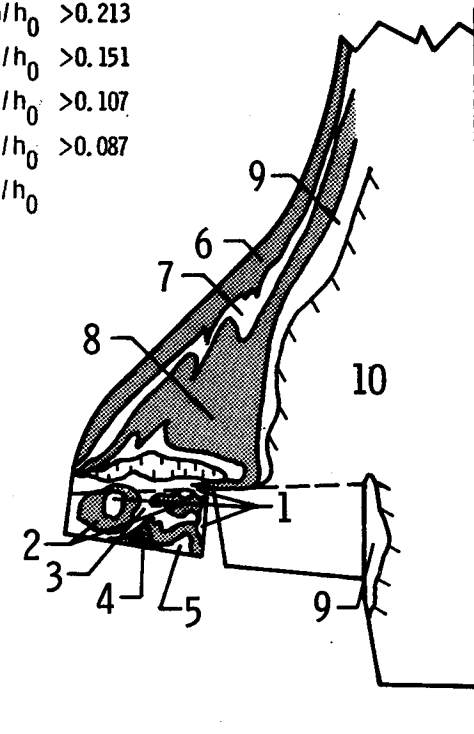
$N_{Re,L} = 0.52 \times 10^6$
$h_0 = 0.059 \, W/cm^2 \, K$

1		h/h_0	> 0.430
2	$0.430 >$	h/h_0	> 0.304
3		h/h_0	> 0.225
4	$0.304 >$	h/h_0	> 0.215
5	$0.225 >$	h/h_0	> 0.159
6	$0.215 >$	h/h_0	> 0.152
7	$0.159 >$	h/h_0	> 0.113
8	$0.152 >$	h/h_0	
9	$0.113 >$	h/h_0	> 0.092
10	$0.092 >$	h/h_0	> 0.080
11	$0.080 >$	h/h_0	
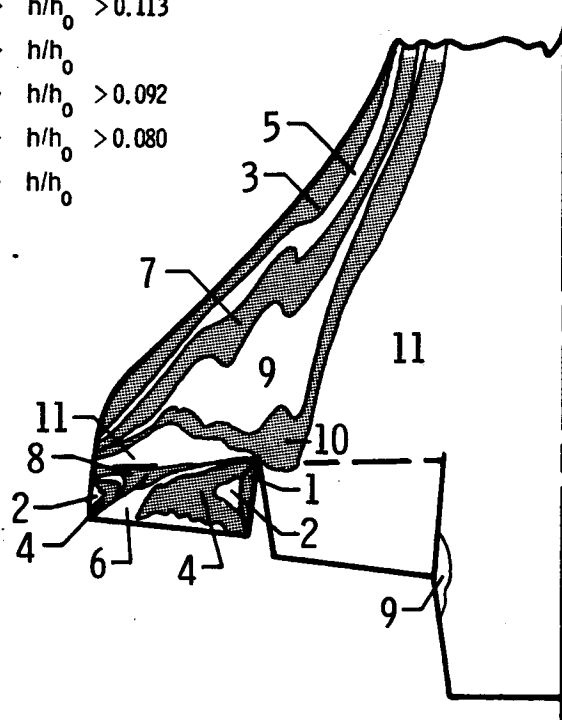
$N_{Re,L} = 2.10 \times 10^6$
$h_0 = 0.114 \, W/cm^2 \, K$

1		h/h_0	> 0.662
2	$0.662 >$	h/h_0	> 0.468
3	$0.468 >$	h/h_0	> 0.331
4	$0.331 >$	h/h_0	> 0.270
5	$0.270 >$	h/h_0	
6		h/h_0	> 0.213
7	$0.213 >$	h/h_0	> 0.151
8	$0.151 >$	h/h_0	> 0.107
9	$0.107 >$	h/h_0	> 0.087
10	$0.087 >$	h/h_0	

(b) $\alpha = 28°$.

Figure 13.- Continued.

13(b)
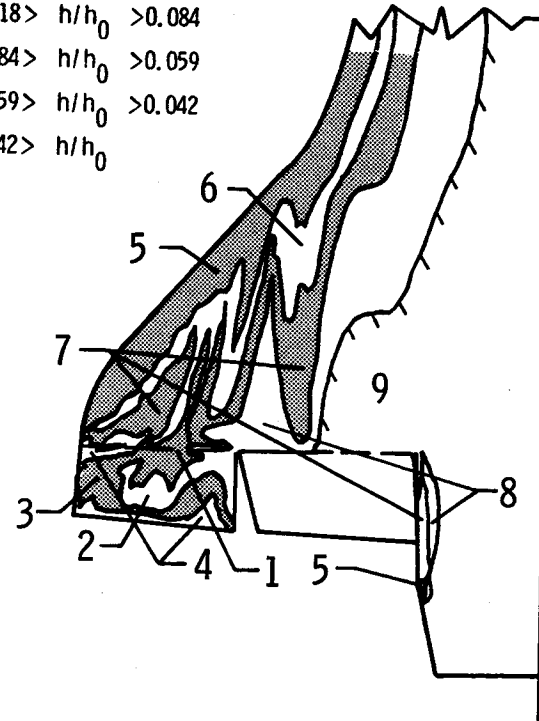
$N_{Re,L} = 0.52 \times 10^6$

$h_0 = 0.059 \, W/cm^2 K$

1		h/h_0	> 0.339
2	$0.339 >$	h/h_0	> 0.240
3	$0.240 >$	h/h_0	> 0.169
4	$0.169 >$	h/h_0	> 0.138
5		h/h_0	> 0.160
6	$0.138 >$	h/h_0	> 0.107
7	$0.160 >$	h/h_0	> 0.113
8	$0.107 >$	h/h_0	
9	$0.113 >$	h/h_0	> 0.080
10	$0.080 >$	h/h_0	> 0.065
11	$0.065 >$	h/h_0	> 0.051
12	$0.051 >$	h/h_0	
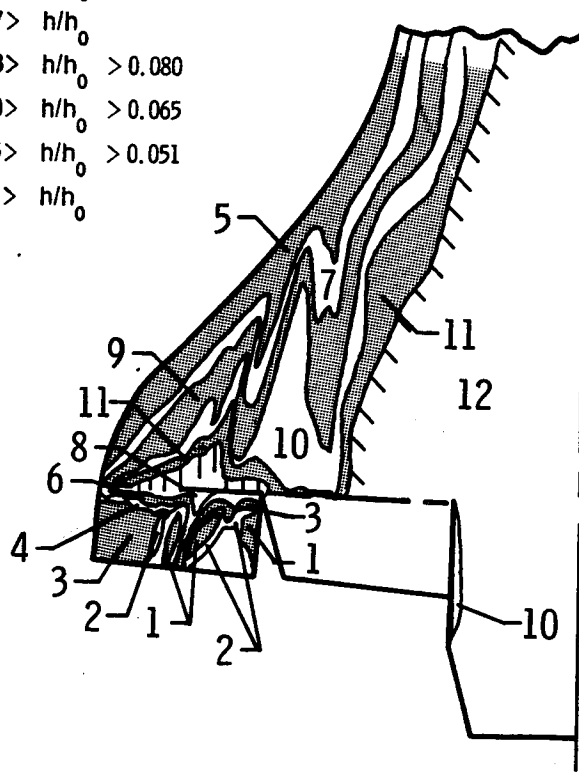
$N_{Re,L} = 2.10 \times 10^6$

$h_0 = 0.114 \, W/cm^2 K$

1		h/h_0	> 0.418
2	$0.418 >$	h/h_0	> 0.296
3	$0.296 >$	h/h_0	> 0.209
4	$0.209 >$	h/h_0	
5		h/h_0	> 0.118
6	$0.118 >$	h/h_0	> 0.084
7	$0.084 >$	h/h_0	> 0.059
8	$0.059 >$	h/h_0	> 0.042
9	$0.042 >$	h/h_0	

(c) $\alpha = 20°$.
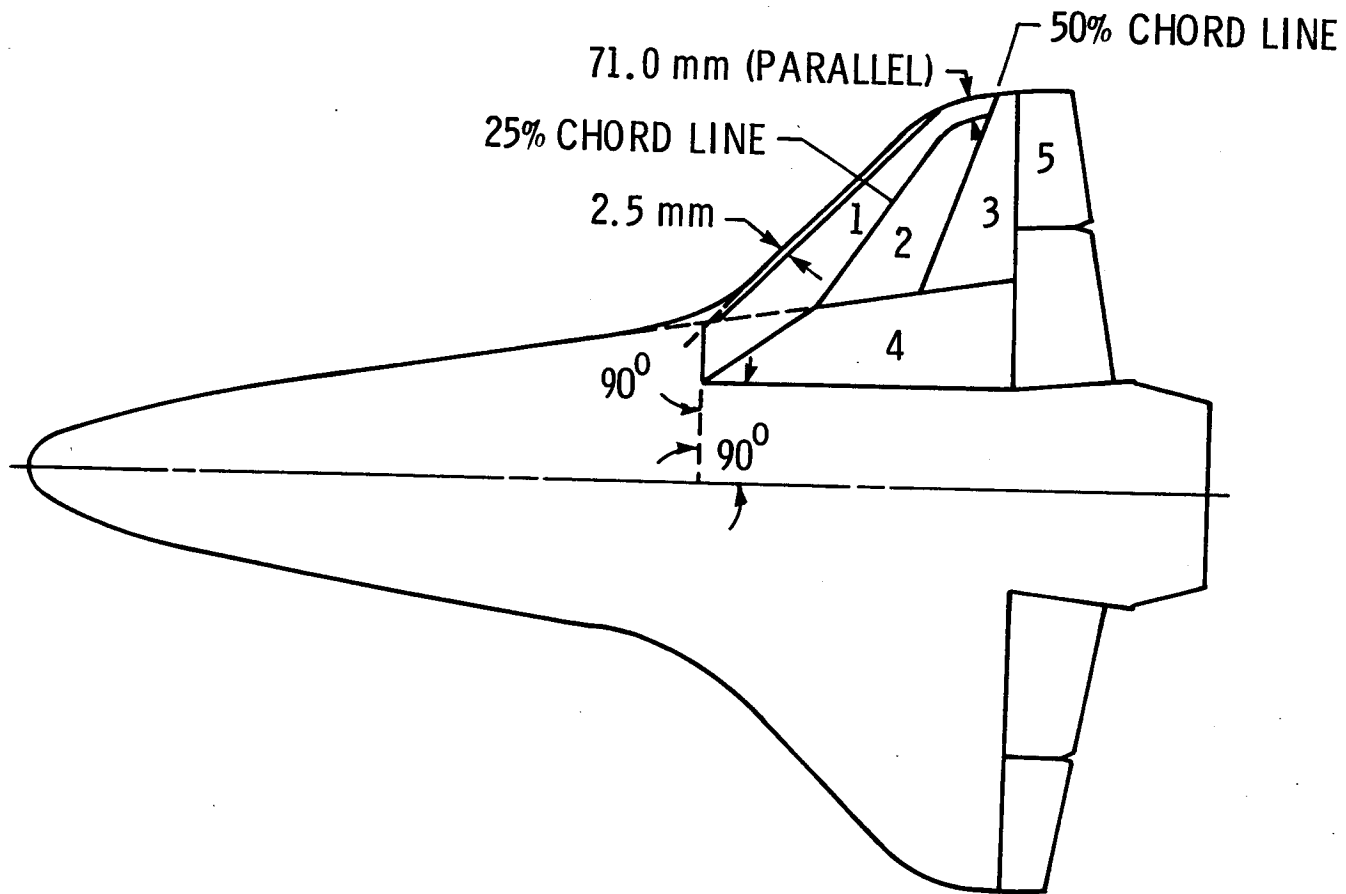
Figure 13.- Concluded.

13(c)

Figure 14.- Location of panels on the orbiter models.
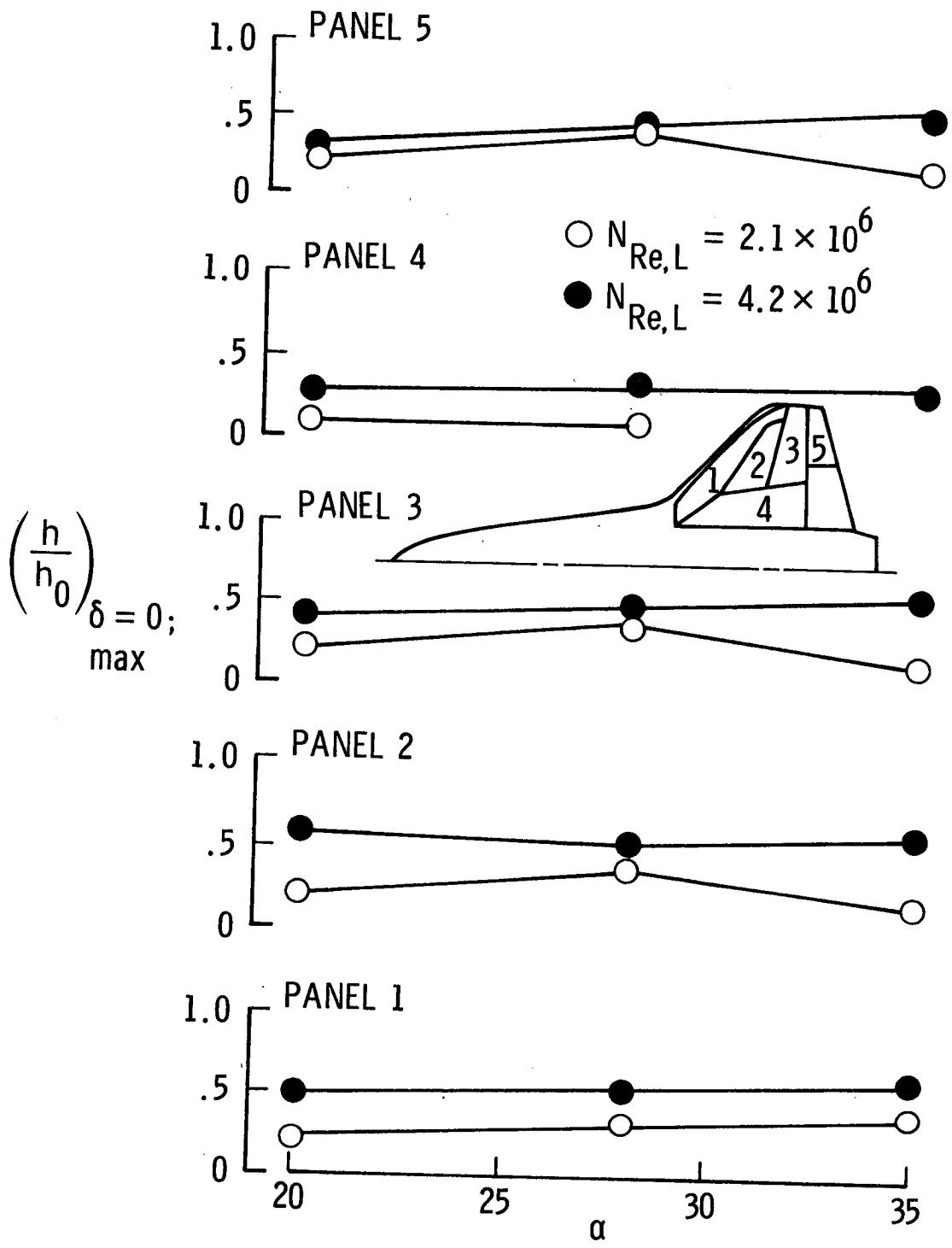
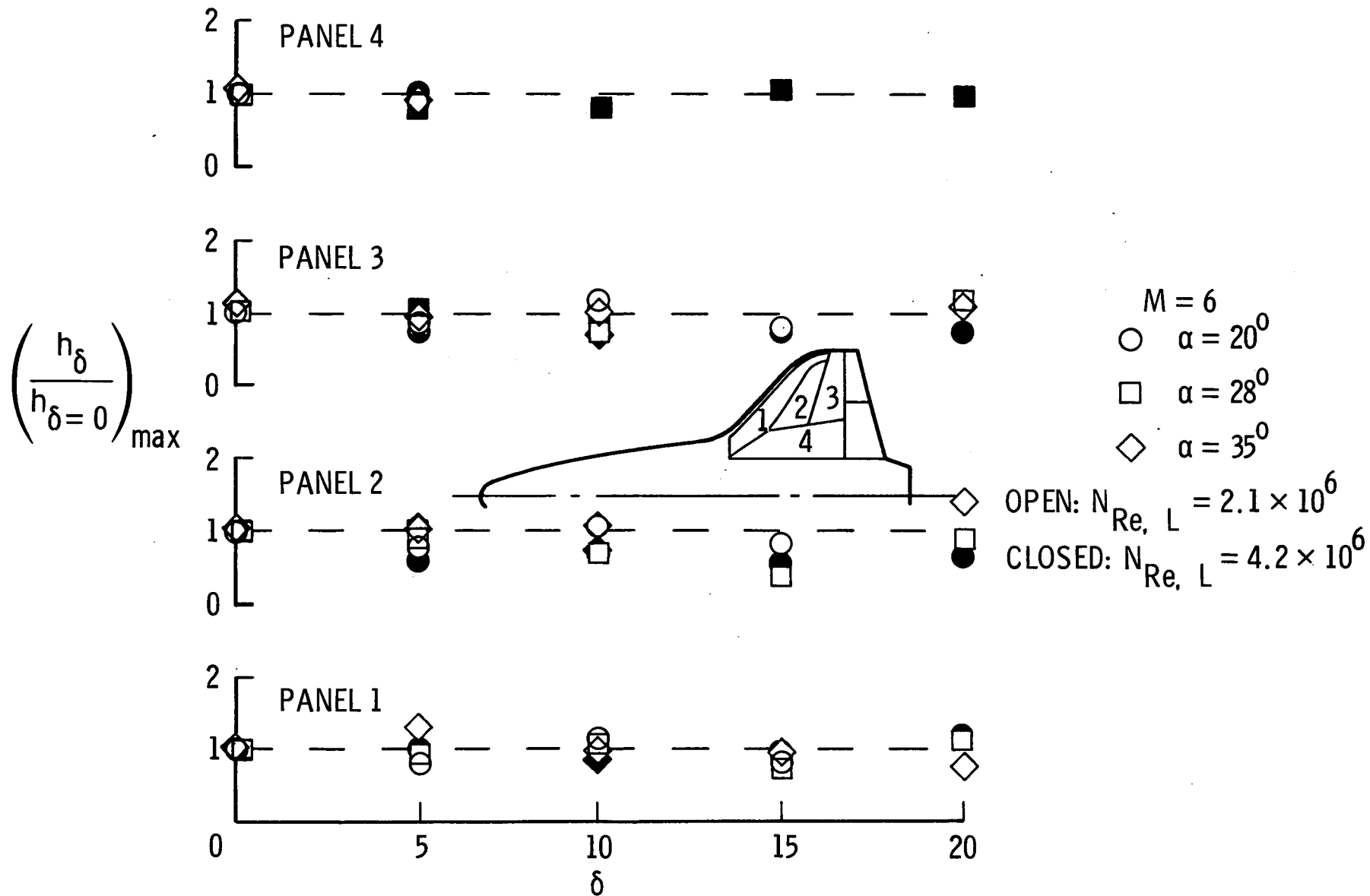Figure 15.– Maximum heat-transfer coefficient that occurs anywhere on each panel when $\delta = 0$ and $M = 6$ at all three α.

PANEL 4

PANEL 3

$\left(\dfrac{h_\delta}{h_{\delta=0}}\right)_{max}$

$M = 6$

○ $\alpha = 20^0$

□ $\alpha = 28^0$

◇ $\alpha = 35^0$

PANEL 2

OPEN: $N_{Re,\ L} = 2.1 \times 10^6$

CLOSED: $N_{Re,\ L} = 4.2 \times 10^6$

PANEL 1

0   5   10   15   20

δ

Figure 16.— Effect of elevon deflection (δ) on the maximum heat-transfer coefficient found anywhere on each of the wing panels when M = 6.
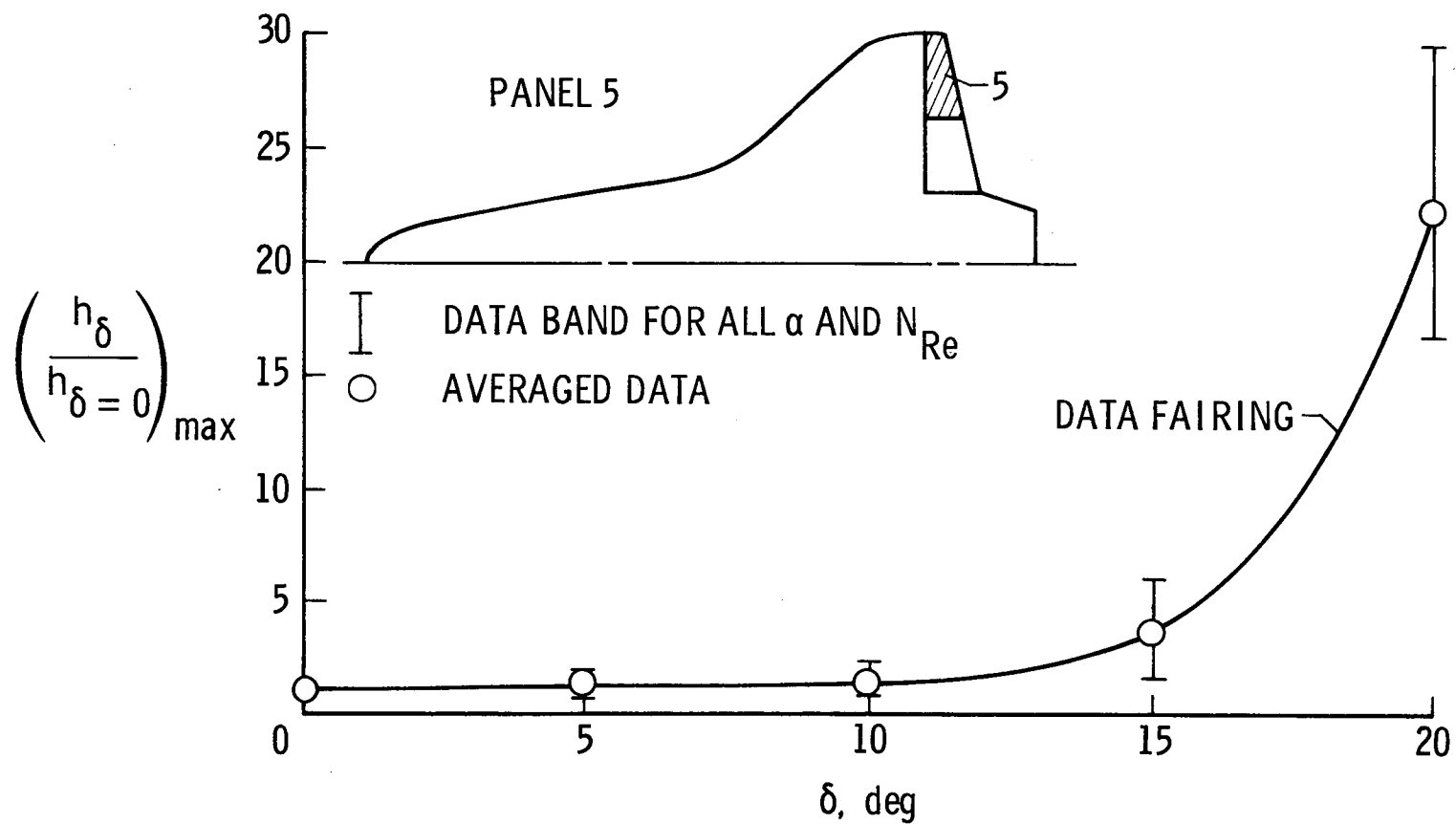
Figure 17.- Effect of elevon deflection (δ) on the maximum heat-transfer coefficient found anywhere on panel 5 (outboard elevon) when M = 6.
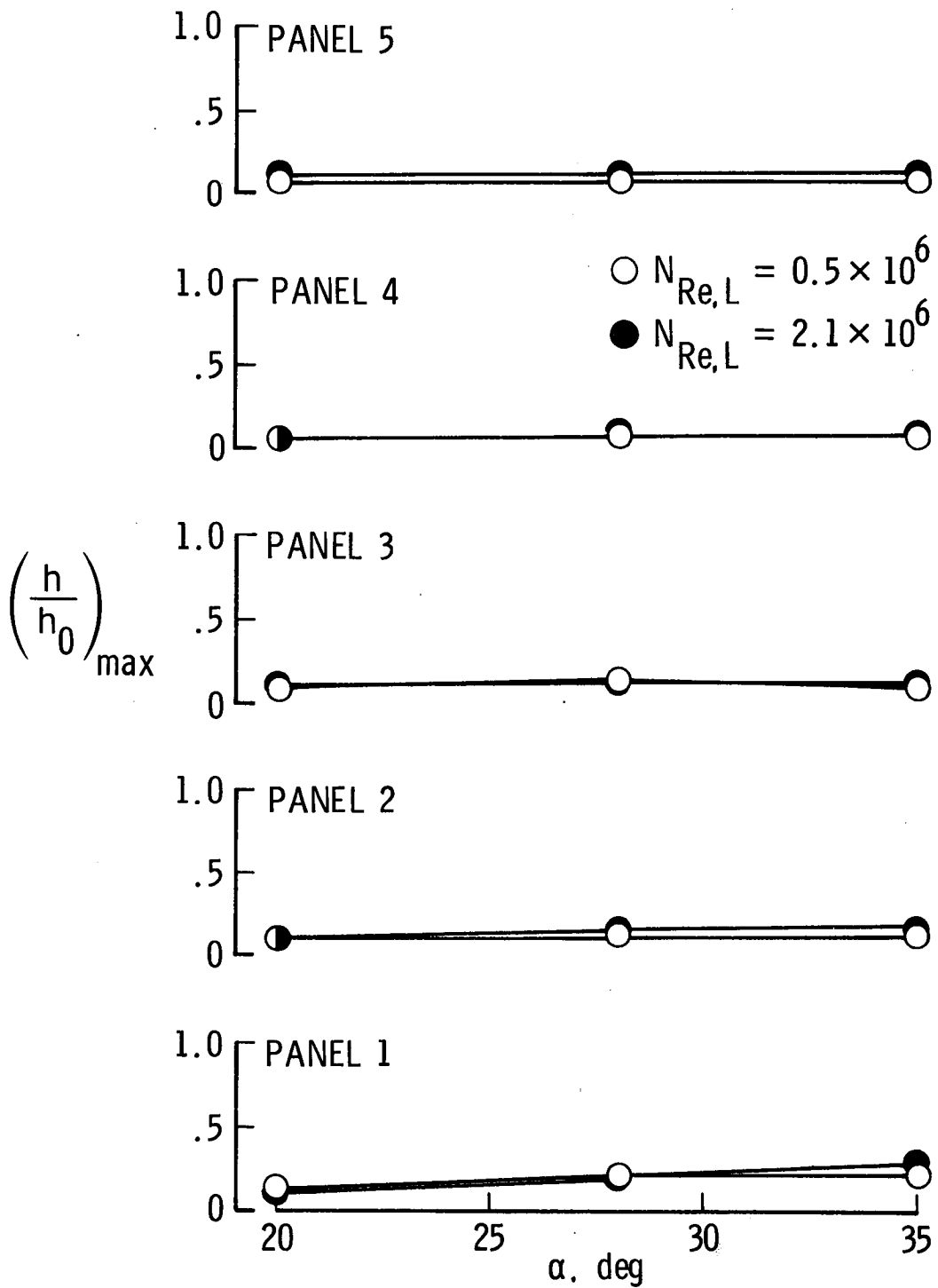
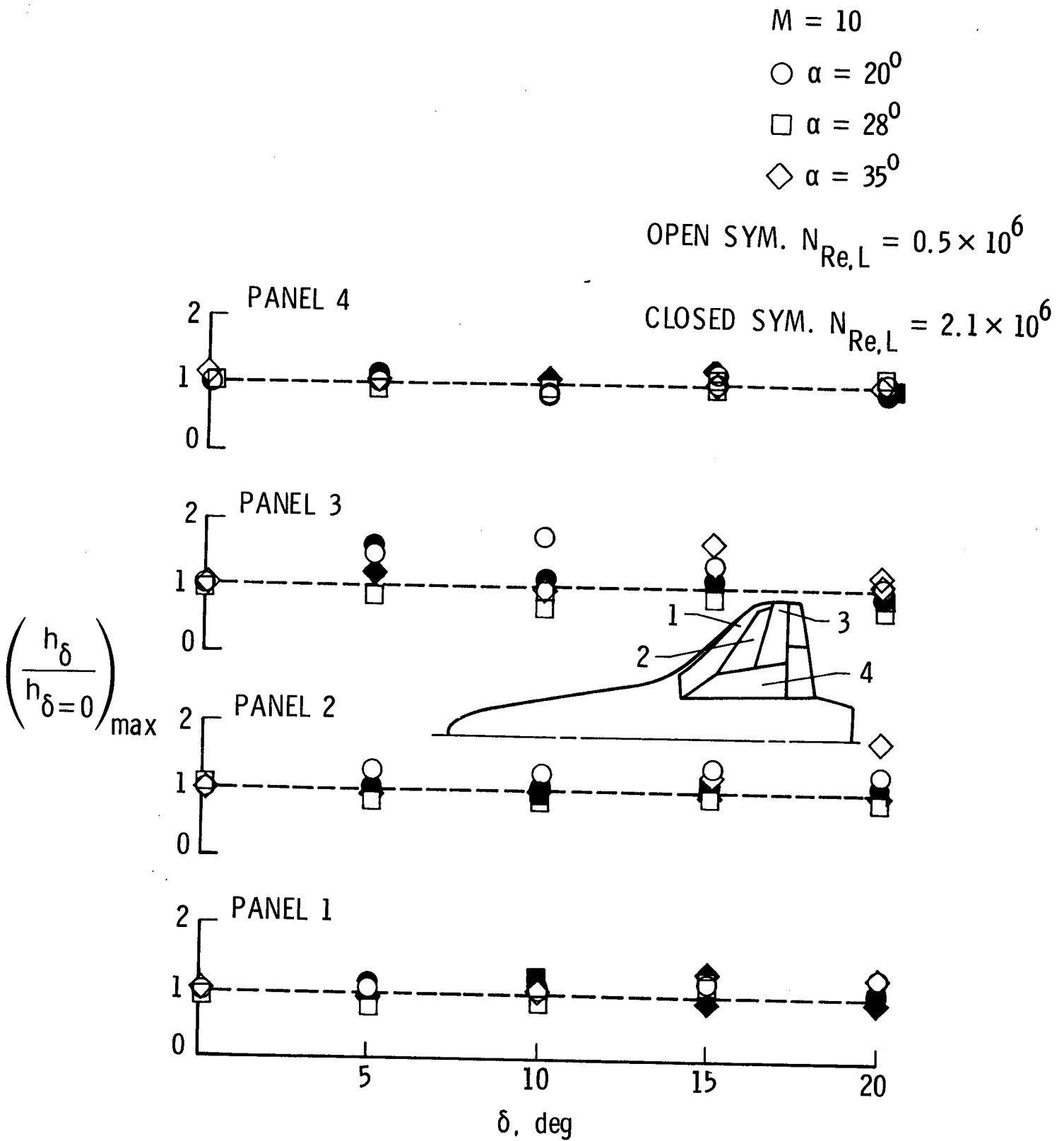Figure 18.- Maximum heat-transfer coefficient that occurs anywhere on each panel when $\delta = 0$ and $M = 10$.

Figure 19.- Effect of elevon deflection (δ) on the maximum heat-transfer coefficient found anywhere on each of the wing panels when M = 10.
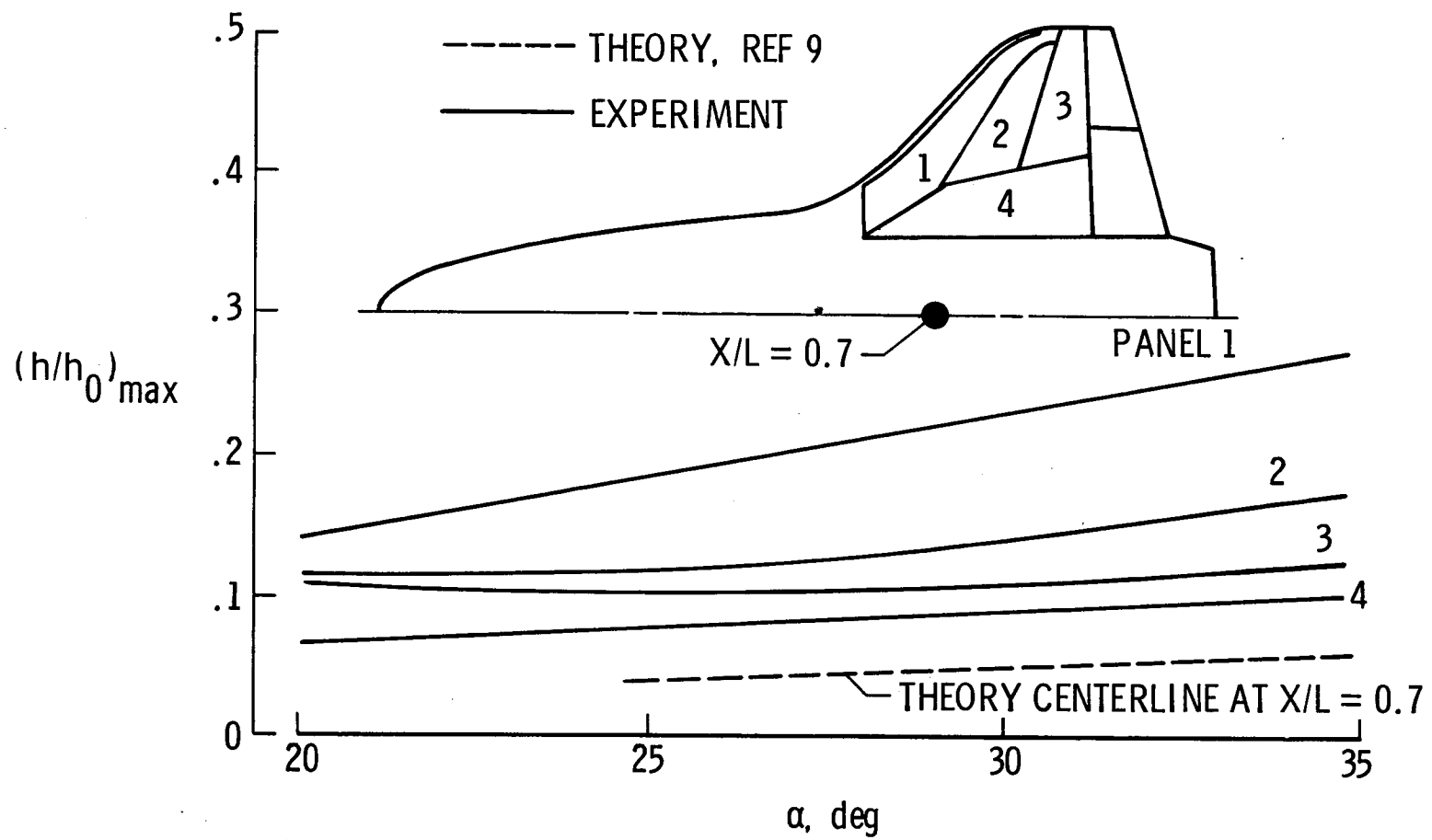
Figure 20.- Comparison of maximum heat-transfer coefficients on all four wing panels and at one point on the orbiter centerline when M = 10.
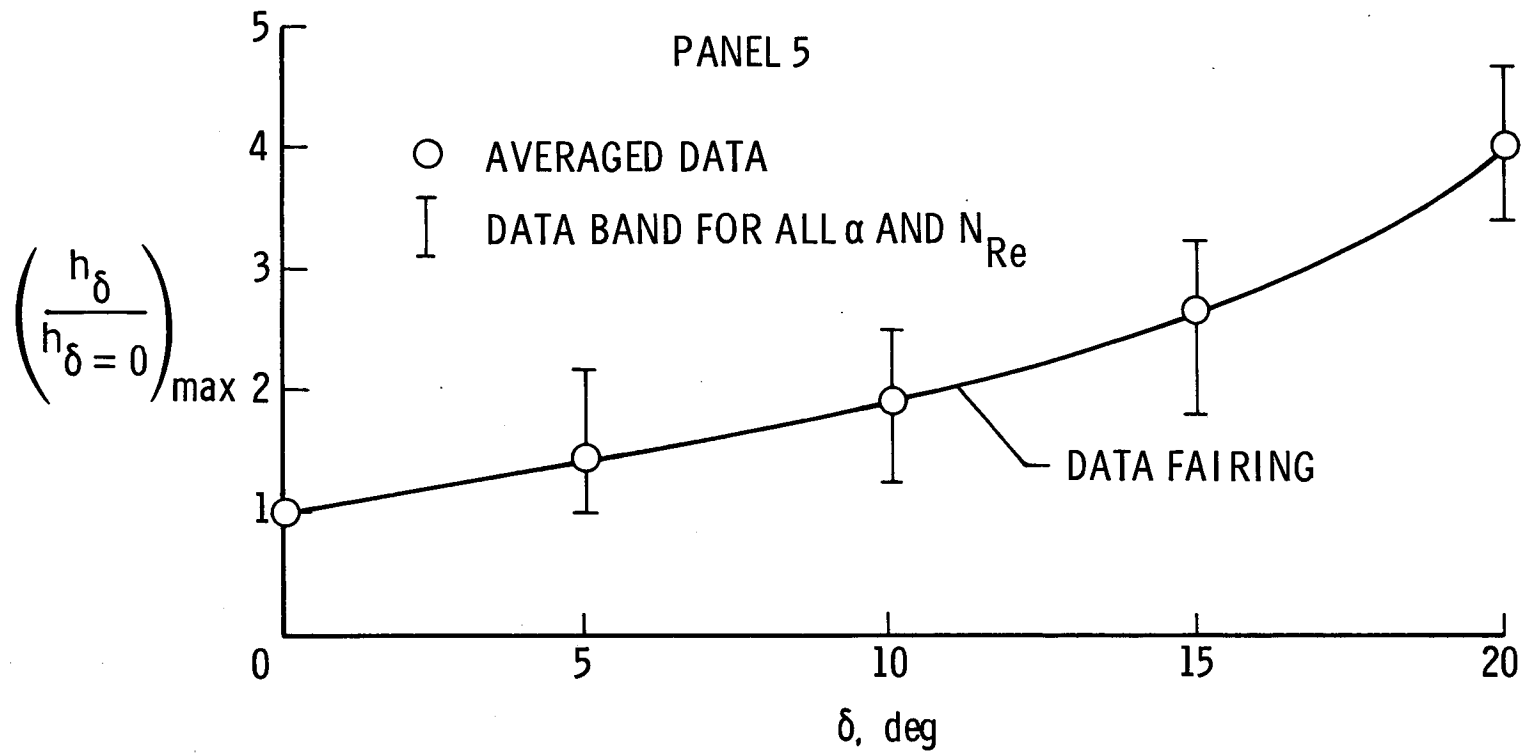
Figure 21.- Effect of elevon deflection (δ) on the maximum heat-transfer coefficient found anywhere on panel 5 (outboard elevon) when M = 10.
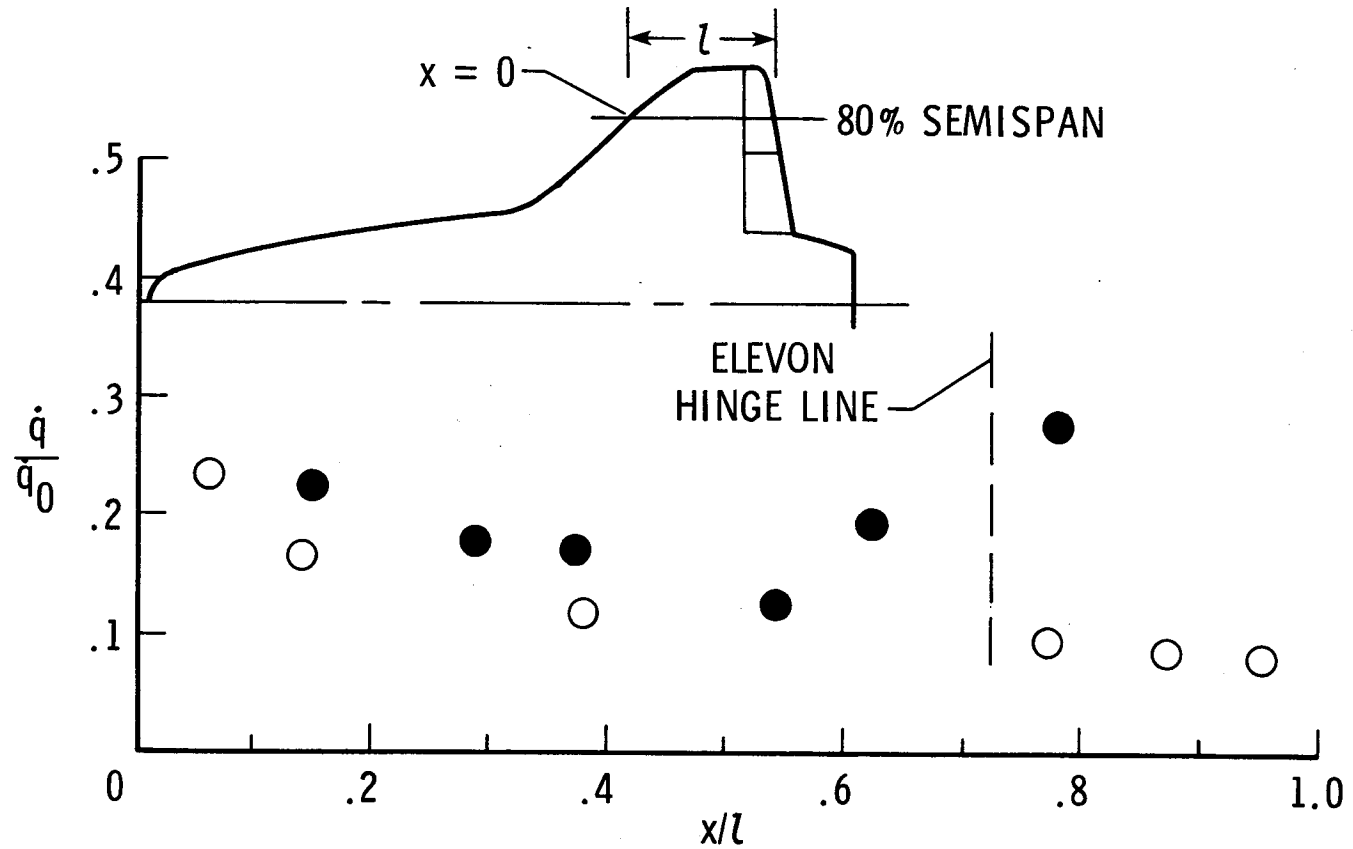
Figure 22.– Comparison of flight (STS-2) and wind-tunnel (Langley CFHT) heat-transfer data.

1. Report No. NASA TM-84646	2. Government Accession No.	3. Recipient's Catalog No.
4. Title and Subtitle Heating Measurements on Space Shuttle Orbiter Models with Differentially Deflected Elevons		5. Report Date May 1983
		6. Performing Organization Code 506-51-13-01
7. Author(s) William L. Wells		8. Performing Organization Report No.
		10. Work Unit No.
9. Performing Organization Name and Address NASA Langley Research Center Hampton, VA 23665		
		11. Contract or Grant No.
12. Sponsoring Agency Name and Address National Aeronautics and Space Administration Washington, D.C. 20546		13. Type of Report and Period Covered Technical Memorandum
		14. Sponsoring Agency Code

15. Supplementary Notes

16. Abstract

The phase-change paint technique was used to make heat-transfer measurements on the windward wing/elevons area of Space Shuttle Orbiter models with differentially deflected elevons. Outboard elevons were deflected windward at angles from $0°$ to $20°$. The inboard elevons were deflected leeward. The models were tested in air at Mach 6 and 10 with two flow conditions and three angles of attack for both Mach numbers. Heat-transfer coefficient contour maps of the wing/elevon area were obtained for all test conditions. The maximum heat-transfer coefficient on the outboard elevon and on certain areas of the wing that were obtained when the elevons were deflected are compared to values obtained when the elevons were undeflected.

17. Key Words (Suggested by Author(s)) Entry Heating Space Shuttle	18. Distribution Statement Unclassified - Unlimited Subject Category 34		
19. Security Classif. (of this report) Unclassified	20. Security Classif. (of this page) Unclassified	21. No. of Pages 61	22. Price A04